OPTIMIZATION OF THE FILAMENT SIZE IN MULTIFILAMENTARY Nb_3Sn SUPERCONDUCTING COMPOSITE

by

SOON-JU KWON
B.S., Seoul National University 1978
M.S., Seoul National University 1980
M.S., Massachusetts Institute of Technology 1982

SUBMITTED TO THE DEPARTMENT OF
MATERIALS SCIENCE AND ENGINEERING
IN PARTIAL FULFILLMENT OF
THE REQUIREMENTS FOR THE DEGREE OF

DOCTOR OF PHILOSOPHY

at the

MASSACHUSETTS INSTITUTE OF TECHNOLOGY
September 1984

Signature of Author.....
Department of Materials Science and Engineering
August 10, 1984

Certified by .....
Robert M. Rose
Thesis Supervisor

Accepted by.....
Bernhardt J. Wuensch, Chairman
Departmental Committee on Graduate Students

OPTIMIZATION OF THE FILAMENT SIZE IN MULTIFILAMENTARY NB_3SN SUPERCONDUCTING COMPOSITE

by

SOON-JU KWON

Submitted to the Department of Materials Science and Engineering on August 10, 1984 in partial fulfillment of the requirements for the degree of Doctor of Philosophy

ABSTRACT

Effects of the filament diameter on the microstructure and the critical current density (J_c) were investigated in the external diffusion processed multifilamentary Nb_3Sn-Cu superconducting composites. J_c was measured in transverse magnetic fields(H) of 10-17 Tesla. The microstructures were examined using scanning electron microscopy (SEM) and transmission electron microscopy (TEM) after each step of the process. Superconducting characteristics were qualitatively rationalized with reference to the microstructures of composites.

The ultrafine filaments (diameter<1μm) had severe shape instability problems (spheroidization and agglomeration) in the thermally activated reaction condition. Filaments of large diameter (>5μm) usually contained unreacted Nb cores with heat treaments typical of commercial materials, so that those composites could not exhibit their full potential. Thus the optimum range of filament diameter was decided to be 1μm-5μm.

Nb_3Sn filaments, when fabricated by one of the conventional diffusional processes, consisted of three concentric shells : the core region with radially directed columnar grains, the outer shell with coarse equiaxed grains, and fine equiaxed grains in the intermediate zone. The columnar structure showed low flux pinning force, due to the orientation of the grain boundary. The coarse grains had low upper critical fields due to the high Sn concentration. The optimum microstructure with the largest volume fraction of equiaxed fine grains might be found in the filament of optimum diameter for a given heat treatment. In such filament the innermost columnar grains barely disappear.

Since most of above phenomena came from the long range diffusional processes of the reaction system, a "diffusionless" powder metallurgical process has been proposed for future work.

Thesis Supervisor : Dr. Robert M. Rose
Title : Professor of Metallurgy

TABLE OF CONTENTS

LIST OF TABLES

LIST OF FIGURES

ACKNOWLEDGEMENTS

Foremost, the author would like to thank professor Robert M. Rose for his humane guidance over the last four years.

Many thanks should be also forwarded to my fellow colleagues -- Dr. Stuart F. Cogan, Dr. James D. Klein and Howard Landis -- for their helpful discussions and laboratorial co-work. The technical assistance of Mr. Irving M. Puffer was indispensable for the completion of this work.

The author wish to extend great appreaciation to his parents, brothers and sisters in Korea for their encouragement throughout all these years. Most importantly, this thesis is dedicated to his beloved wife Soon-Myung H. Kwon, whom he married recently.

This work was supported by the US Department of Energy through the MIT Plasma Fusion Center.

I. Introduction

Superconducting materials are currently applied to many fields ranging from micro-switching devices to fusion confinement magnet coils. Almost all of the large-scale applications require the superconducting materials in the form of wire to transmit the electrical current (or eventually to produce a magnetic field). Consequently, the processing technology of wire fabrication is very important in the practical application of a superconducting material.

Nb_3Sn wire was fabricated by Kunzler et al[1] in 1961 using powder metallurgy and sustained more than $10^5 A/cm^2$ in 8.8 Tesla (= 88 KGauss). This was a milestone for the high-current high-field application of superconducting compounds.

However, a monolithic superconducting wire like the above tends to become normal far below the expected maximum operating condition. This is due to the heat produced inside the superconductor due to mechanical disturbances and/or flux jumping during operation [2,3]. If a small region of a superconductor is subjected to mechanical disturbances and/or a flux jump, energy is released. A fraction of the energy is dissipated as heat. In certain circumstances the heat can be enough to quench the small volume to the normal state. Since the normal state resistance of a superconductor is very high, the small normal region causes intense local heating. This is followed by quenching of the surrounding area into the normal state. Once the transition takes place in a small region, the entire wire, without appropriate heat dissipation devices, quenches into the normal state catastrophically. This is known as the instability problem.

To avoid the instabilities, one should design a wire (1) to reduce the amount of heat released (2) to increase the capability of heat dissipation from the normal region. The latter can be achieved by cladding the superconductor with a low electrical and low thermal resistance normal conductor, such as copper. On the other hand, it is known that the amount of heat coming out from the unit volume of a superconductor is proportional to the diameter of the conducting filament[2,3]. As a result, a multifilamentary composite with a good normal conducting matrix is the most accepted geometry of a superconducting wire.

After the monolithic Nb_3Sn wire mentioned above, considering the instability problem, there have been developed and improved various processing techniques to make multifilamentary Nb_3Sn composite. These are the bronze process[4], external diffusion process[5], in-situ process[6,7], Sn-core process[8-10], jelly-roll process[11,12], etc.. The critical current densities (J_c's) of some of those wires exceed the order of $10^5 A/cm^2$ in the magnetic field of 12 Tesla.

In any process, the critical current density of a composite is a function of many variables -- e.g. the filament/matrix volume ratio, the concentration of Sn, the heat treatment schedule, the filament diameter, etc.. To date, most of the research has been performed on the effects of the heat treatment schedule and the Sn concentration. However, to specify the optimum filament diameter in a composite design, one should have information on the size effect. Thus, the primary purpose of this research was set to obtain the information -- e.g. How does the filament diameter affect the microstructure, and how

does the microstructure have influence on the critical current density of a composite.

To determine the optimum filament diameter, there are two strategies which contradict each other : one tends to reduce the filament size, the other to enlarge the filament size(Fig. 1.1).

Reasons for the former strategy are as follows;

(1) Once a small amount of transport current starts to flow inside the superconductor placed in an applied magnetic field of between H_{c1} and H_{c2}, the magnetic flux lines move due to the Lorentz force. The flux lines meet defects and are pinned by them[2]. When the Lorentz force exceeds the pinning force, the unpinned flux lines move, producing resistance heating to quench the superconductor into normal state.

In Nb_3Sn, the grain boundary is believed to be the most effective flux pinning center [13]. Many attempts have been directed at the understanding of the relationship between the grain size and the flux pinning force density [13-16]. T. Luhman has summarized that the critical current density is inversely propotional to the grain size of Nb_3Sn until the grain become less than 300-500A [17]. One of the processing ideas to achieve such a grain size was to suppress the growth of the Nb_3Sn grains by reducing the diameter of the original Nb filament to the comparable dimension. This idea leads to the fabrication of a ultrafine filamentary composite in which the nominal filament diameter is order of 1000A or less.

(2) A more basic argument for the ultrafine filamentary composite is the dependence of current carrying capacity on the strain. Due to

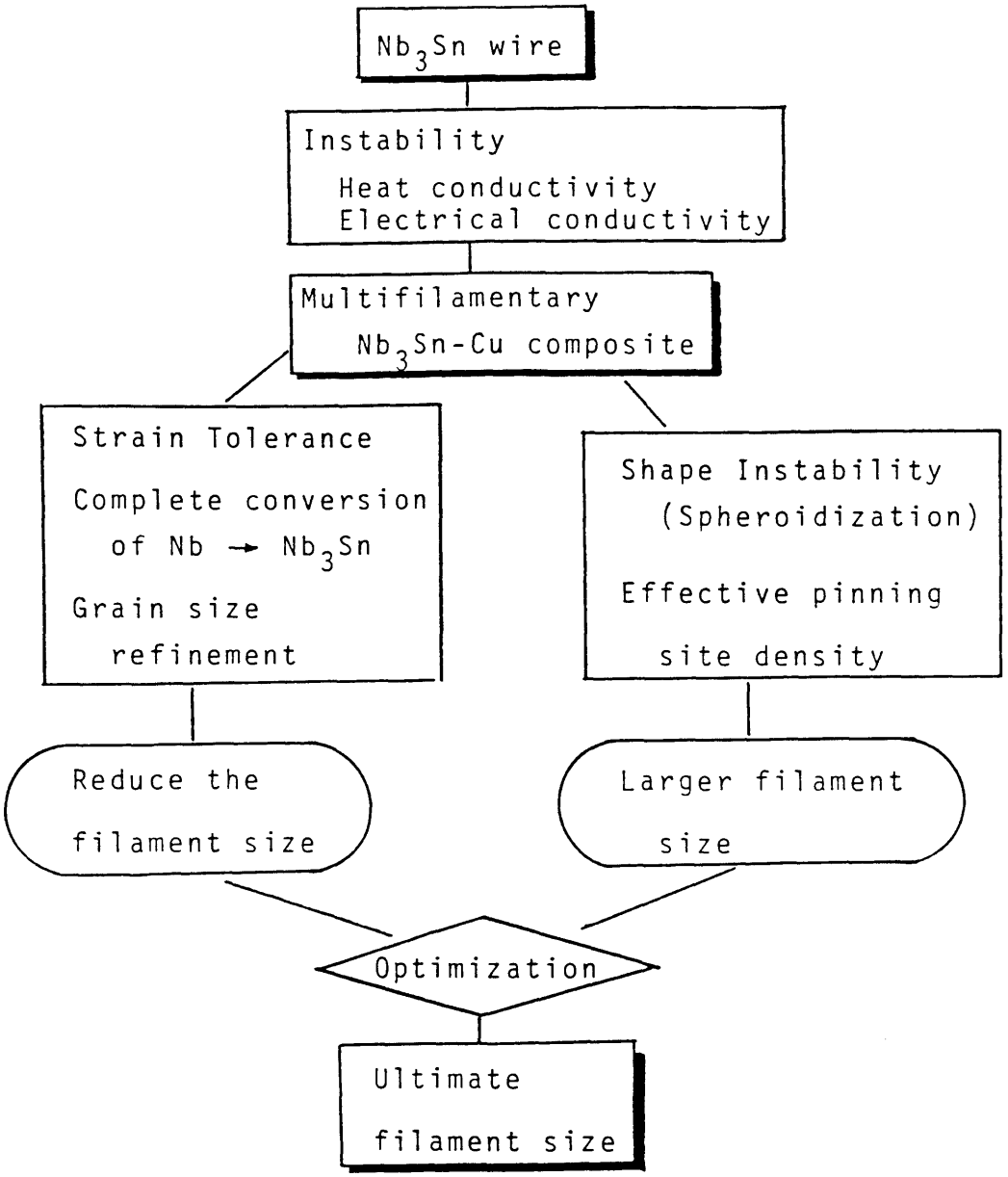

Fig. 1.1 Strategy of the Nb_3Sn superconducting wire design

the high Lorentz force, the magnet coil experiences large radial forces which result in tension on the wire. Large strains in a filament will degrade the current carrying capacity[18-20]. There is a strong indication that the strain tolerance can be increased by reducing the filament size and the local Nb_3Sn to matrix ratio[21]. This will increase the compressional pre-strain, developed during the Nb_3Sn formation reaction, on the superconducting filament and make the wire sustain higher tensile strain without appreciable degradation in the critical current density.

(3) If a filament size increase beyond a certain dimension, only a fraction of the Nb filament will be converted to the Nb_3Sn, for a reasonable heat treatment which does not greatly increase the grain size of Nb_3Sn. The critical current density of such composite is evidently lower than that of smaller filament composite in which the whole Nb has been converted to the superconducting phase.

On the other hand, the reasons to pursue larger filament size are as follows;

(1) If a filament size is very fine, the filaments subject to shape instability under heat treatment. This leads to the spheroidization of filaments and electrical discontinuity, which will decrease the current carrying capacity of the wire. This phenomenon will be discussed in detail in Chapter IV of this article.

(2) As the diameter of the filament decreases, the interfacial area between the superconducting phase and the normal phase will increase at expense of the grain boundary area of the superconducting phase. When the filament diameter is almost the same as that of Nb_3Sn

grains, the density of volume flux pinning site (grain boundary area per unit volume of Nb_3Sn) will be quite low. Since one filament is formed by mono-chain of grains.

Consequently, as shown in Fig.1.1, there should be an attempt to optimize the filament size to design a superconducting composite of best performance. In this research, the effect of the filament size has been studied for the optimization. Data of composites with a wide range of filament diameter have been compiled from the literature and the present experiment. The existence of the optimum range of filament diameter was confirmed from the data, and explained in terms of the structural instability and the existence of unreacted Nb core in a filament. Within the optimum range, the general trend of the dependence of the critical current density on the filament diameter was derived and also explained in terms of the microstructures of the superconducting phase.

II. Materials

Since the primary purpose of this research is the determination of the optimum filamet size Nb_3Sn superconducting wire, composite wires were carefully selected and/or fabricated to have various filament size. The smallest filament size was about 0.1μm and the largest one was about 15μm. The specifications of the composites are listed in Table 2.1.

The 61 and 61^2(=3721) filament composites

These composites were fabricated by the tubing and bundling technique. The process starts with swaging of an OFHC copper tube onto a Nb rod. This single core composite was drawn down through hexagonal dies. The hexagonal wire was cut into pieces and 61 pieces were hex-packed in an OFHC copper tube. This 61-filament composite was swaged and drawn down to 6.35mm diameter, and divided into two sections; one for drawing down to 61-filament composites of various diameters, and the other for drawing through hexagonal dies and restacking to have 61^2(=3721) filaments. The latter was reduced to the same overall diameters as the former. By appropriately etching out the surface Cu tube, the volume % of Nb was controlled. The 61-filament composite has 28 volume % of Nb. There are two kinds of 61^2-filament composites; one has 25 volume % Nb, the other 40 volume % Nb. Details of the fabrication processing of these composites have been published elsewhere[21].

Typical cross-sectional appearance of the 61^2-filament composite is shown in Fig. 2.1(a). The primary 61-filament colonies are also

Table 2.1 Specification of composites

Composite*	Vol.% Nb**	Wire dia.(mm)+	Fila. dia.(μm)++
61-17	28	0.254	17
2K-3	28	0.254	3
61^2-2.9	40	0.277	2.87
61^2-2	25	0.254	2
61^2-1.8	40	0.173	1.8
2K-1.5	28	0.124	1.5
61^2-1.4	25	0.173	1.4
61^2-1.3	40	0.124	1.3
61^2-1	25	0.124	1
0.8M-0.1	20	0.254	0.1
1.7M-0.09	23	0.254	0.09

* The labels stand for the specifications of materials as follow ; (No. of filament)-(Nominal diameter of filament in μm unit) e.g. 1.7M-0.09 composite contains 1.7 million filaments of 0.09μm nominal diameter.

** After the Sn plating and reaction heat treatment the Vol.% of Nb_3Sn may be different from the initial vol.% Nb. However, it was assumed that the volume % do not change.

\+ These values will change after the reaction heat treatment about 10% due to the externally incoporated Sn.

++ Calculated from the data -- No. of filaments, vol.% of filament, and wire diameter -- listed in the previous three columns.

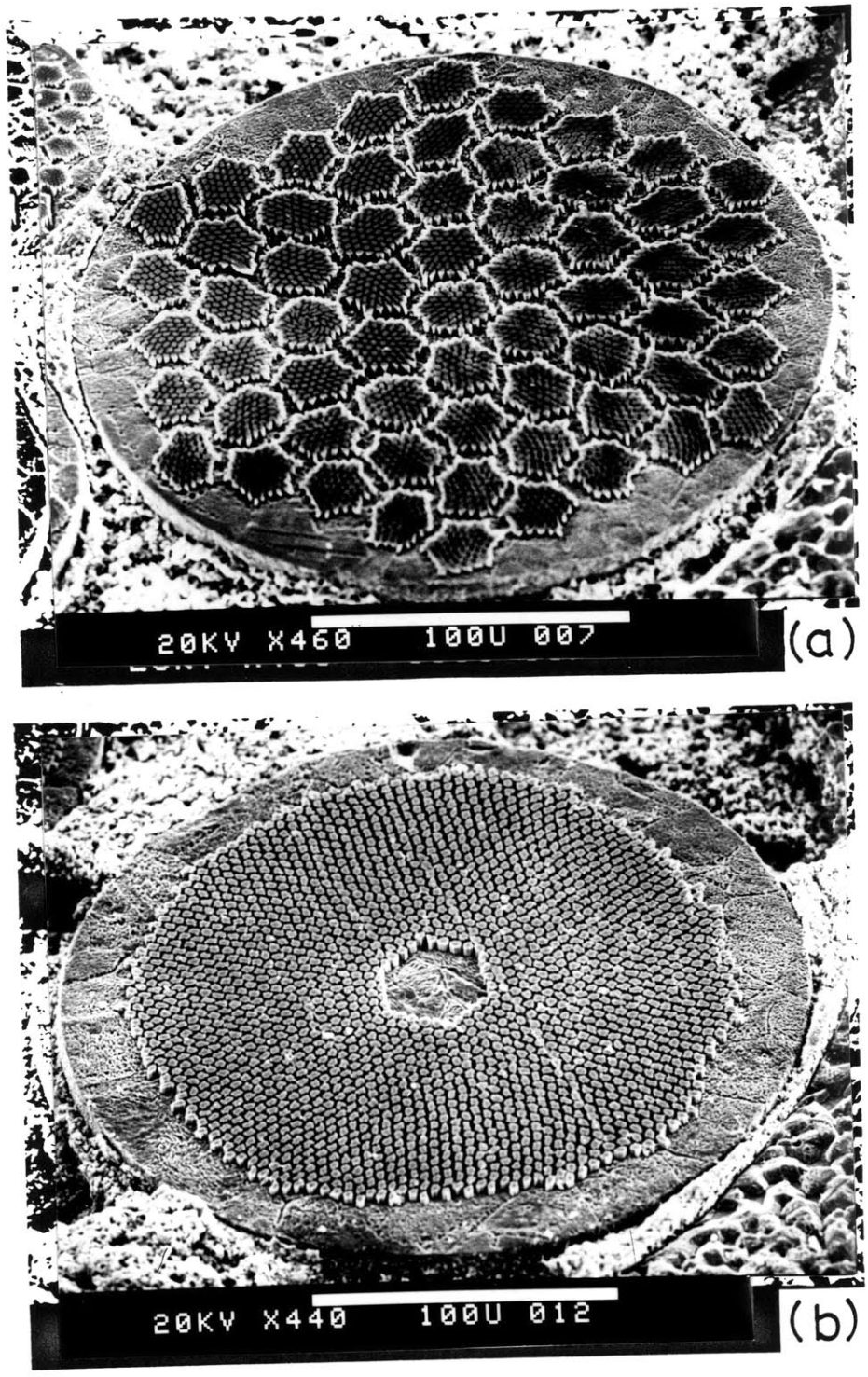

Fig. 2.1 The cross-sections of as-drawn composites.
(a) 61^2(=3721) filaments. Composite dia. = 0.254mm
(b) 1956 filaments. Composite dia. = 0.254mm

shown in the SEM micrograph. When the diameter of the 28 volume % 61-filament composite is 0.254mm, the nominal diameter of each filament is 17μm. In case of the 40 volume % 61^2-filament composites, when the composite diameters are 0.254mm, 0.173mm, and 0.124mm, the nominal filament diameters are 2.6μm, 1.8μm and 1.3μm, respectively. For the 25 volume % 61-filament composites of same diameters, those are 2μm, 1.4μm and 1μm, respectively.

The 2K(1956)- and 1.7M-filament composites

The fabrication process of these composites begins with drilling 1956 holes in an OFHC copper rod. Swaging and drawing down to the wire form with 1956 Nb filaments in the holes results in the apprearance shown in Fig. 2.1(b).

The nominal filament diameters are 3.04μm, 2.06μm and 1.49μm for the composite diameters of 0.254mm, 0.173mm and 0.124mm, respectively. All these wires have 28 volume % of Nb.

The 0.254mm diameter composite was fabricated by the IGC (Intermagnetic Coperation), and the composites of smaller diameters were drawn down to the respective final dimensions in this laboratory.

At an intermediate stage of the 2K composite fabrication, a portion of the wire was cut into pieces and hex-packed to have 1.7×10^6 Nb filaments. This 1.7M-filament composite has 23 volume% of Nb and 0.09μm of nominal filament diameter when the wire diameter is 0.254mm.

0.8M filaments composite

This composite was produced by the same technique as the previous 1.7M-filament composite. On a 152.4mm diameter OFHC billet, 1148 holes of 1.6mm diameter were drilled for Nb. The Cu-Nb composite billet was extruded to the diameter of 3.2mm and 709 pieces of this composite were stacked in a 76.2mm diameter Cu tube. It was extruded and drawn down to 0.254mm diameter wire and 0.1μm of nominal filament diameter.

III. EXPERIMENT

3.1. General

The overall scheme of this research is shown in Figure 3.1.1.

Inspection of the as-drawn composite : The cross-sectional and longitudinal appearance of the as-drawn Nb-Cu composites were inspected under SEM in order to characterize those wires. Detailed sample preparation technique is given in the section 5 of this chapter.

Pre-annealing - A solution heat treatment : The characterized wires were cut into several 20cm-long pieces. Solution heat treatment was performed on these wires for 16 hours at 650°C and 10^{-5} torr to eliminate the heterogeneous nucleation sites for porosity. Such porosity tends to form during the reaction heat treatment step[21].

The pre-annealed wires were brought to SEM to look into the cross-sectional and longitudinal morphology. Sample preparation technique of these wires was the same as that of as-drawn wires.

Sn plating : Sn was electroplated on the pre-annealed wire from a commercially available Stannous Fluoborate solution. The composition is given elsewhere [22]. A low current density ($30mA/cm^2$) was employed in order to control the amount of Sn plated as precisely as possible.

The amount of Sn to be plated was decided on the basis of the weight % of residual Sn in the matrix after the complete conversion of Nb to Nb_3Sn. The goals were 2 weight % or 5 weight % of residual Sn in the bronze matrix. The weight of Sn was about 10mg for a 0.254mm-diameter 20cm-long Nb-Cu composite and about 2.5 mg for a 0.127mm-diameter one. The quantity of Sn plated was measured with a sensitive double-pan chain balance and controlled within 5% error.

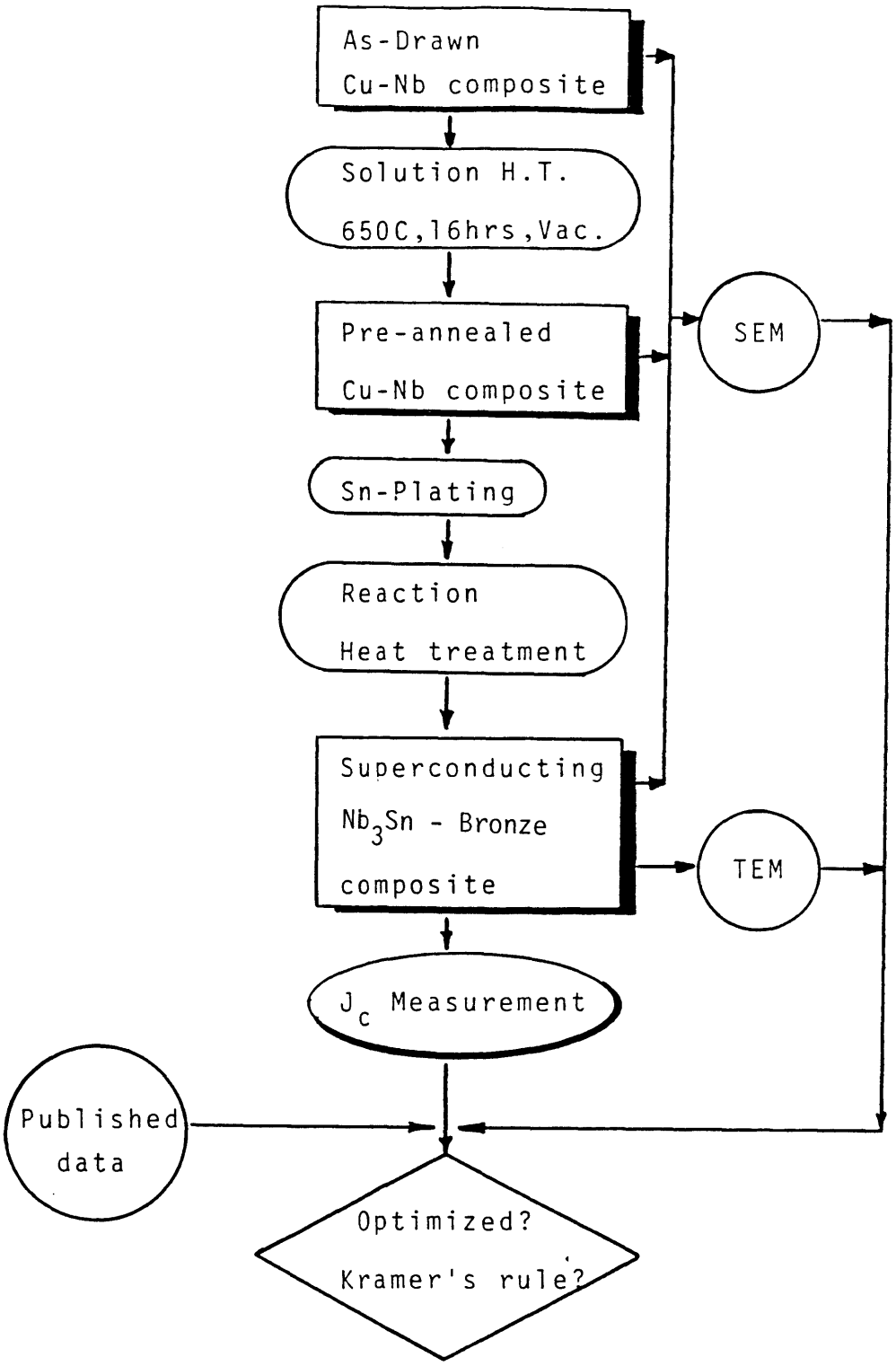

Fig. 3.1.1 Overall scheme of the present research

Sn diffusion heat treatment : Due to the large difference between the melting point of Sn(232°C) and the reaction temperature (550°C - 800°C), special care should be taken to avoid problems -- such as, beading, delamination, formation of porosities, etc. Based on the previous diffusion kinetics study in the Cu-Sn binary system[22], a successful heat treatment schedule was established to overcome the difficulties.

A typical diffusion heat treatment schedule for a 0.254mm-diameter composite is shown in Fig.3.1.2. There are several important points to be mentioned in this schedule -- (i) As the temperature approaches 220°C*, the ramping rate should be decreased in order to avoid unexpected overheating above the melting point of Sn, due to the surplus heat from rapid ramping. (ii) Temperature should be kept at 220°C* as long as possible. At this stage, a large proportion of Sn will be transformed into ϵ- and η-phase. (iii) Within the temperature range of 220°C-240°C, the ramping rate should be extremely slow. At this stage, one might take the advantage of unavoidable temperature fluctuations and gradients, introducing a situation similar to the zone melting. Only a part of Sn might be in the molten state, and the rest of the solid phase would partially support the melt, avoiding beading and instability of the molten layer.

Reaction heat treatment : After the temperature went up to the range where the formation of Nb_3Sn is possible, various heat treatment schedules were applied according to the purpose of each experiment. To

* 220°C was chosen to avoid accidental liquefaction of the Sn due to temperature fluctuations of the furnace.

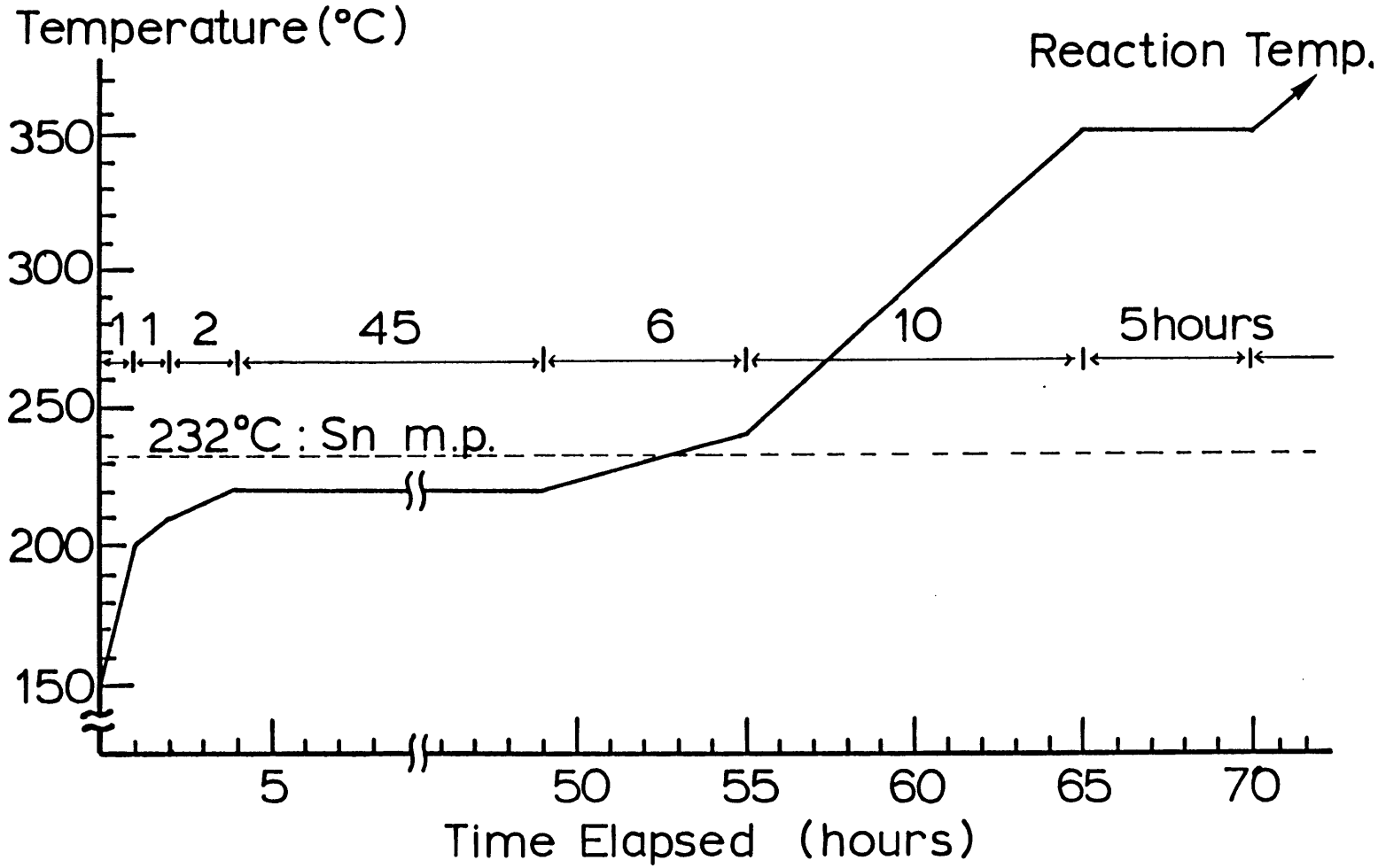

Fig. 3.1.2 Typical example of a diffusion heat treatment schedule for a 0.254mm dia. composite

study the effect of filament size, one batch of heat treatment (192 hours at 650°C + 22hours at 750°C) was applied for the set of composites of interest. For other sets, time scanning was performed to study the effect of heat treatment period.

The reacted superconducting Nb_3Sn-Bronze composite was then prepared for SEM and TEM examinations. The critical current was measured as described in the following section.

3.2 Critical current measurement

Critical current(I_c) was measured in a transverse magnetic field with the standard-four-point probe technique. The experimental set-up is illustrated in Fig.3.2.1. The magnetic field was generated within a 5cm-diameter Bitter solenoid at the Francis Bitter National Magnet Laboratory.

The voltage drop was measured across 1 cm of the superconducting wire, using a Keithley Nanovoltmeter. A criterion of 1μV/cm voltage drop was used to determine the superconducting to normal transition. When the charge carriers (electron pairs in superconducting state, free electrons in normal state) pass through the sample, the transverse magnetic induction B in the sample interacts with the carriers to exert the Lorentz force (F=JxB) on the carriers and to the sample itself. The direction of transporting direct current was chosen, so that sample deformation due to the Lorentz force could be prevented by a supporting plate.

The current and the voltage leads were soldered to the sample using 60Sn-40Pb alloy. Extreme care was taken to minimize damage to the

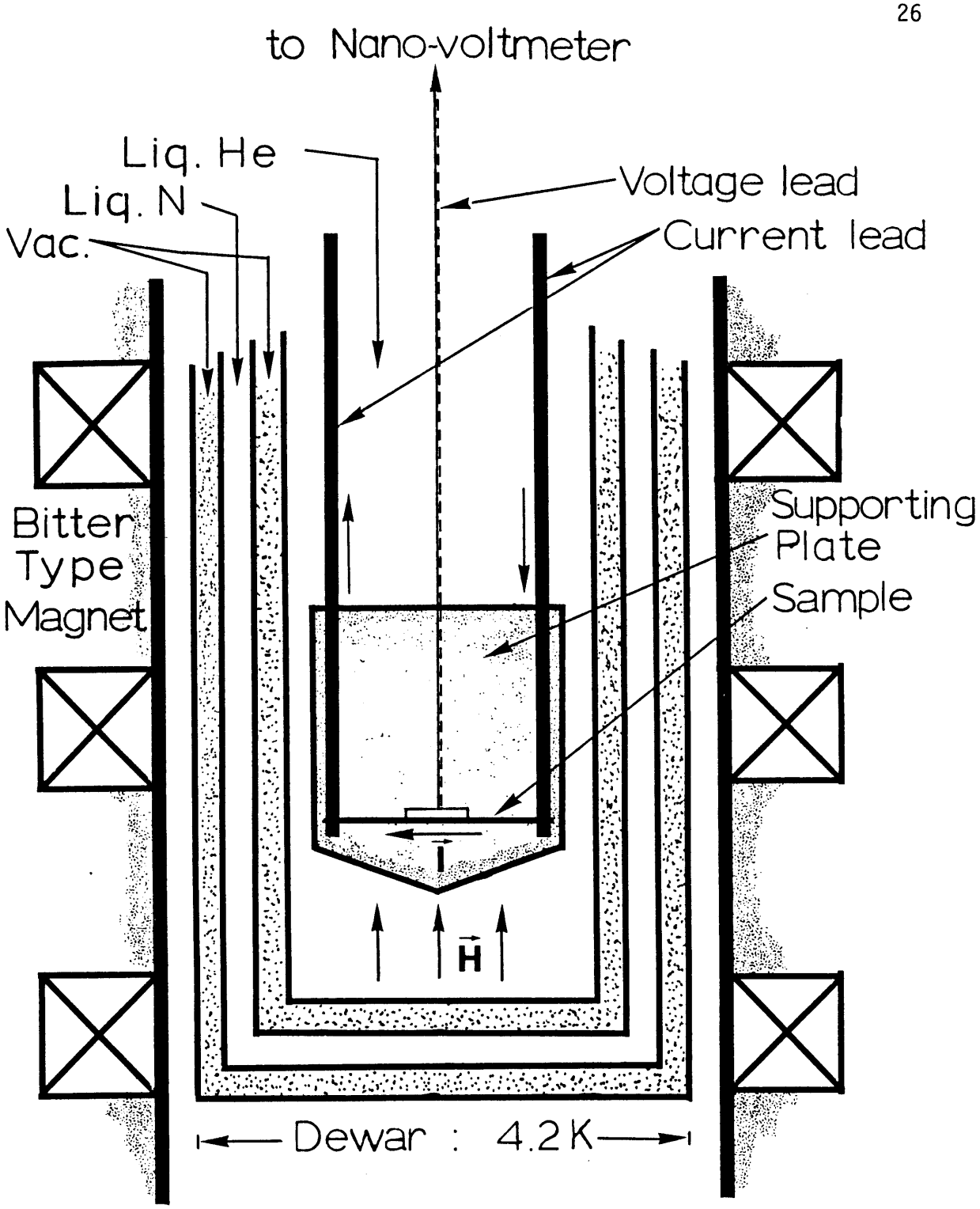

Critical current measurement set-up

Fig. 3.2.1

sample. Even though this sample mounting method is generally accepted, a certain degree of damage is inevitable from the surface melting of wire to make good contact.

3.3. Scanning Electron Microscopy

Sample preparation methods depended on the purpose of the examination.

For the observation of surface morphology of a filament, a 5 mm long piece was cut from the wire. One end of the piece was immersed in aqueous 1:1 HNO_3 solution, and the bronze (or Cu) matrix was dissolved out to reveal the bare Nb_3Sn (or Nb) filament. It was rinsed with methanol and dried completely. The piece was laid on the special stub for the SEM. The unetched end was fixed on the stub using a conductive silver paint.

To get cross-sectional information, the wire was soldered into a small hole machined with a precision drill in a 12.5mm-diameter 5mm-height brass button. The mounted sample was then ground and polished using conventional metallographic technique. To make the surface relief appropriate for SEM examination, the polished cross-section of composite was etched collectively. To relieve the filaments, the bronze (or Cu) matrix was etched with a solution of 55 ml HPO_4, 25 ml CH_3COOH and 20 ml HNO_3. The reacted Nb_3Sn layer was etched using a solution of 20 ml HF, 15 ml H_2SO_4, 5 ml HNO_3 and 50 ml H_2O.

Since scanning electron microscopy requires a conductive surface, every specimen was coated with a thin layer of gold using a vacuum

evaporation apparatus. Those samples were examined with an AMR or a Cambridge scanning electron microscope operated at 20KV.

3.4. Transmission Electron Microscopy

The TEM sample was prepared with following procedure (refer to Fig.3.4.1) ;

On a 600 mesh emery paper, the opposite sides of a piece of composite wire (2.5cm-long) was ground in longitudinal direction to make a ribbon of 50μm thickness. The width of the ribbon was same as the diameter of the original composite (Fig. 3.4.1). 2.5mm-long pieces were cut from the ribbon using a surgical blade on a microscopic watch glass. Special care was taken to minimize the strain damaged area of the specimen. Two of such pieces were mounted parallel to each other on a 3mm-diameter Cu grid having a 1mm-diameter concentric hole. A Cu powder dispersed adhesive was used to fix the specimen on the grid.

The specimen was then electro-jet polished in a solution of 93% methanol, 2% HF, 5% H_2SO_4 at -50°C, employing 25V and 30mA. The speed of jet flow was controlled, so that the flows injected horizontally from the opposite nozzles (about 1.5cm apart) meet at the centered sample location without deflecting vertically. The electro-jet polishing was performed until the specimen piece has a very narrow neck. Final thinning was done in an argon ion bombardment chamber operated at 5KV, 0.5mA with a gun angle of 12°. Even though such a deliberate procedure was employed, it was very difficult to obtain sufficient width and thinness for TEM work.

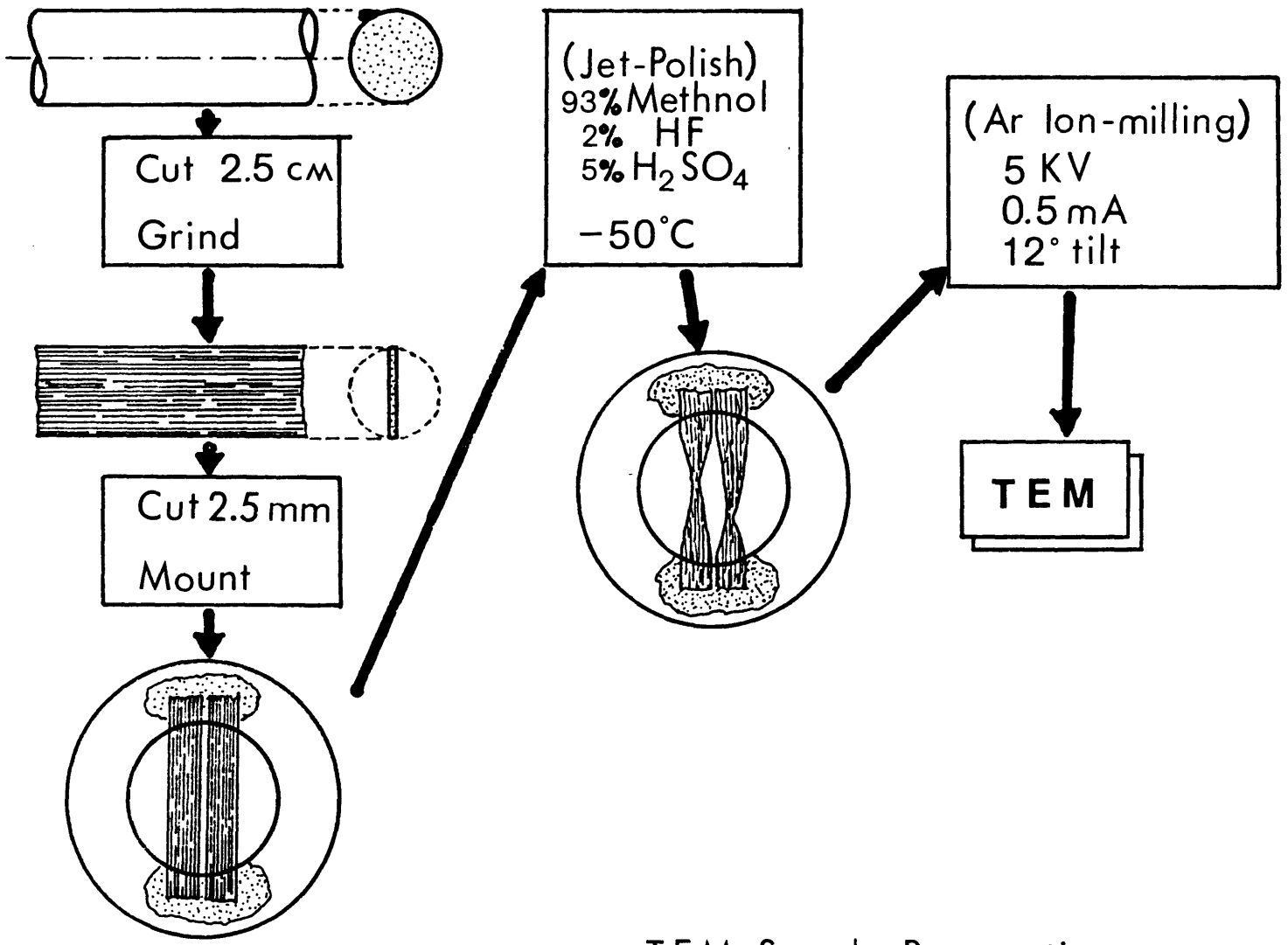

Fig. 3.4.1 TEM Sample Preparation

The internal structure of the thinned specimen was then examined in a Philips EM300 transmission electron microscope with 100KV accelerating voltage.

IV. RESULTS

4.1 Critical Current Density (J_c)

The critical current density over the entire cross-section of a composite is widely used to represent the property of the wire. However this is not an appropriate parameter to understand the filament size effect with composites of various volume fraction of filaments. Rather the critical current density over the filament cross-section is more appropriate. In the present research, all the critical current densities are calculated for the unit cross-sectional area of the filament.

The critical currents of the composites, measured in transverse magnetic fields of 10-17 Tesla, are listed in Table 4.1.1. The related critical current densities are tabulated (Table 4.1.2), and plotted as a function of the applied magnetic field (Fig. 4.1.1).

The ultrafine filamentary composite (1.7M-0.09) showed quite low critical current density (J_c). The 61^2-2 composite had unexpectedly low J_c compared to other composites of similar filament size, especially at low field. The surface color of this wire indicated that there was insufficient amount of Sn for the complete reaction of the filament to Nb_3Sn. A cross-sectional examination of this wire revealed that there was a large area of unreacted Nb at the core of a filament.

The effect of filament size was not clearly visible in this plot (Fig. 4.1.1). Therefore the J_c of each material was normalized with respect to that of a reference. Since there was no standard material, the author believed that the composite with the best performance in this research (i.e. 61^2-1.8) was the most appropriate choice as the

Table 4.1.1 Critical current (I_c) measured in transverse magnetic fields

(unit : 1 Amp)

Composite*	Heat treatment**	12T	13T	14T	15T	16T	17T
61-17	(1)	9.6	8.4	7.1	6.1	5.5	-
2K-3	(2)	36	26.7	17	9.3	5.34	2.56
61^2-2.9	(2)	60.8	40.8	25.9	14.4	7.0	3.2
61^2-2	(2)	14.6	10.5	6.8	4.3	2.11	1.29
61^2-1.8	(2)	36.7	22	13.2	7	3.7	1.56
2K-1.5	(2)	11.1	7.3	3.8	2.2	1.16	0.48
61^2-1.4	(2)	9.6	6.5	3.9	1.8	0.74	0.28
61^2-1.3	(2)	10.55	6.6	3.95	1.94	0.86	0.34
61^2-1	(2)	5.55	3.44	1.9	0.93	0.36	0.16
1.7M-0.09***	(3)	8.5	5.19	2.79	1.38	0.54	-
0.8M-0.1	(4)	1.06	-	0.12	-	-	-

* The labels define the specification of composite as follow ;
(No. of filament)-(Nominal diameter of filament in μm unit)
e.g. 1.7M-0.09 composite contains 1.7 million filaments of 0.09μm nominal diameter.

** Heat treatment : (1) 750°C, 60hours
(2) (650°C,192hours)+(750°C,22hours)
(3) 600°C,375hours
(4) 750°C, 60hours

*** I_c = 14.2 Amp at 11 Tesla

Table 4.1.2 Critical current density (J_c) over the unit cross-sectional area of filaments

(unit : $10^3 Amp/cm^2$)

Composite*	12T	13T	14T	15T	16T	17T
61-17	67.9	58.9	50.0	42.9	37.5	-
2K-3	202.3	149.8	95.5	52.3	30.0	14.4
61^2-2.9	164.6	110.5	70.1	39.0	19.0	8.7
61^2-2	110.8	80.0	51.6	32.6	16.0	7.6
61^2-1.8	297.6	178.4	107.0	56.8	30.0	12.7
2K-1.5	278.5	183.2	95.4	55.2	29.1	12.0
61^2-1.4	134.7	91.2	54.7	25.3	10.4	3.9
61^2-1.3	160.2	100.2	60.0	29.5	13.1	5.2
61^2-1	144.8	89.8	49.6	24.3	9.4	4.2
1.7M-0.09**	73.0	44.6	23.9	11.8	4.6	-
0.8M-0.1	7.0	-	0.8	-	-	-

* The labels define the specifications of composites as follow ; (No. of filament)-(Nominal diameter of filament in μm unit) e.g. 1.7M-0.09 composite contains 1.7 million filaments of 0.09μm nominal diameter.

** $J_c = 13.2 \times 10^3$ amp/cm^2 at 11 Tesla

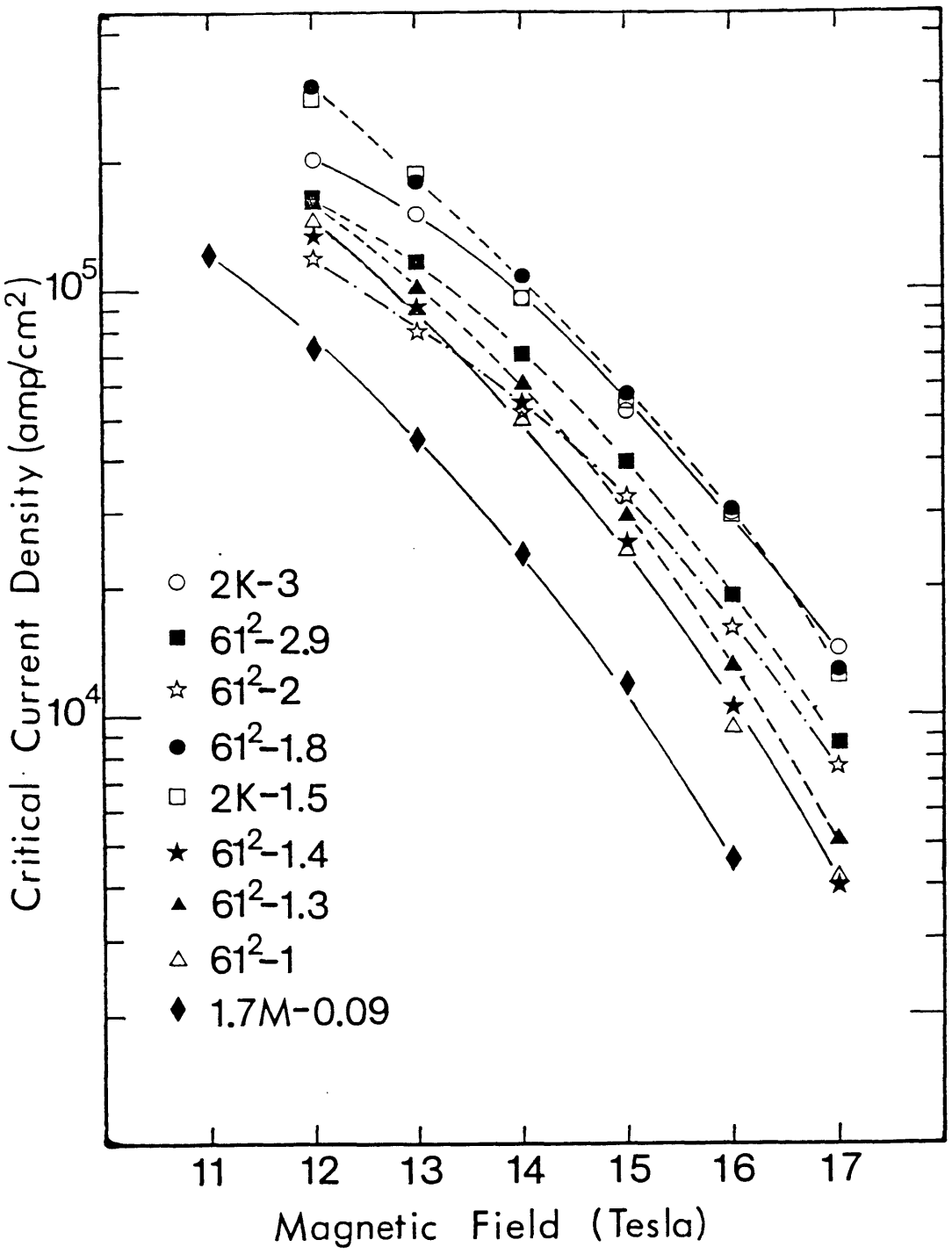

Fig. 4.1.1 Critical current density (J_c) measured in transverse applied magnetic field.

note : Composites are defined as follow;
(No. of filament)-(Nominal diameter of filament in μm unit)
e.g. 1.7M-0.09 composite contains 1.7 million filaments of 0.09μm nominal diameter.

reference. The normalized J_c's with respect to the 61^2-1.8 composite are listed in Table 4.1.3. Using the least-square-method, best fitting lines were drawn for each composite in a normalized J_c versus applied magnetic field plot (Fig. 4.1.2).

In this illustration, one might notice that the slope of the best fitting line is positive, when the diameter of filament is larger than 1.8μm. The slope becomes negative for the filament smaller than 1.8μm in diameter. Generally the slope increases as the filament diameter increase. To visualize the trend more clearly, the slopes of the lines were plotted with respect to the filament diameter as shown in Fig. 4.1.3. Then the dependence of the critical current density on the filament size might be stated as follow :

> Large filament diameter has a detrimental effect on the low field J_c. Small filament diameter produced low J_c, especially in the high fields.

The above statement will be supported through the discussion of the microstructure.

Table 4.1.3 Normalized J_c's with respect to the 61^2-1.8 composite

Composite*	12T	13T	14T	15T	16T	17T
2K-3	0.680	0.840	0.893	0.921	1	1.134
61^2-2.9	0.553	0.619	0.655	0.687	0.632	0.682
61^2-2	0.372	0.448	0.482	0.574	0.533	0.598
61^2-1.8	1	1	1	1	1	1
2K-1.5	0.936	1.027	0.891	0.972	0.970	0.948
61^2-1.4	0.453	0.511	0.511	0.446	0.347	0.307
61^2-1.3	0.538	0.562	0.561	0.519	0.435	0.406
61^2-1	0.487	0.503	0.463	0.428	0.313	0.329
1.7M-0.09	0.245	0.253	0.223	0.208	0.154	-

* The label defines the specification of a composite as follow;
(No. of filament)-(Nominal diameter of filament in μm unit)
e.g. 1.7M-0.09 composite contains 1.7 million filaments of 0.09μm nominal diameter.

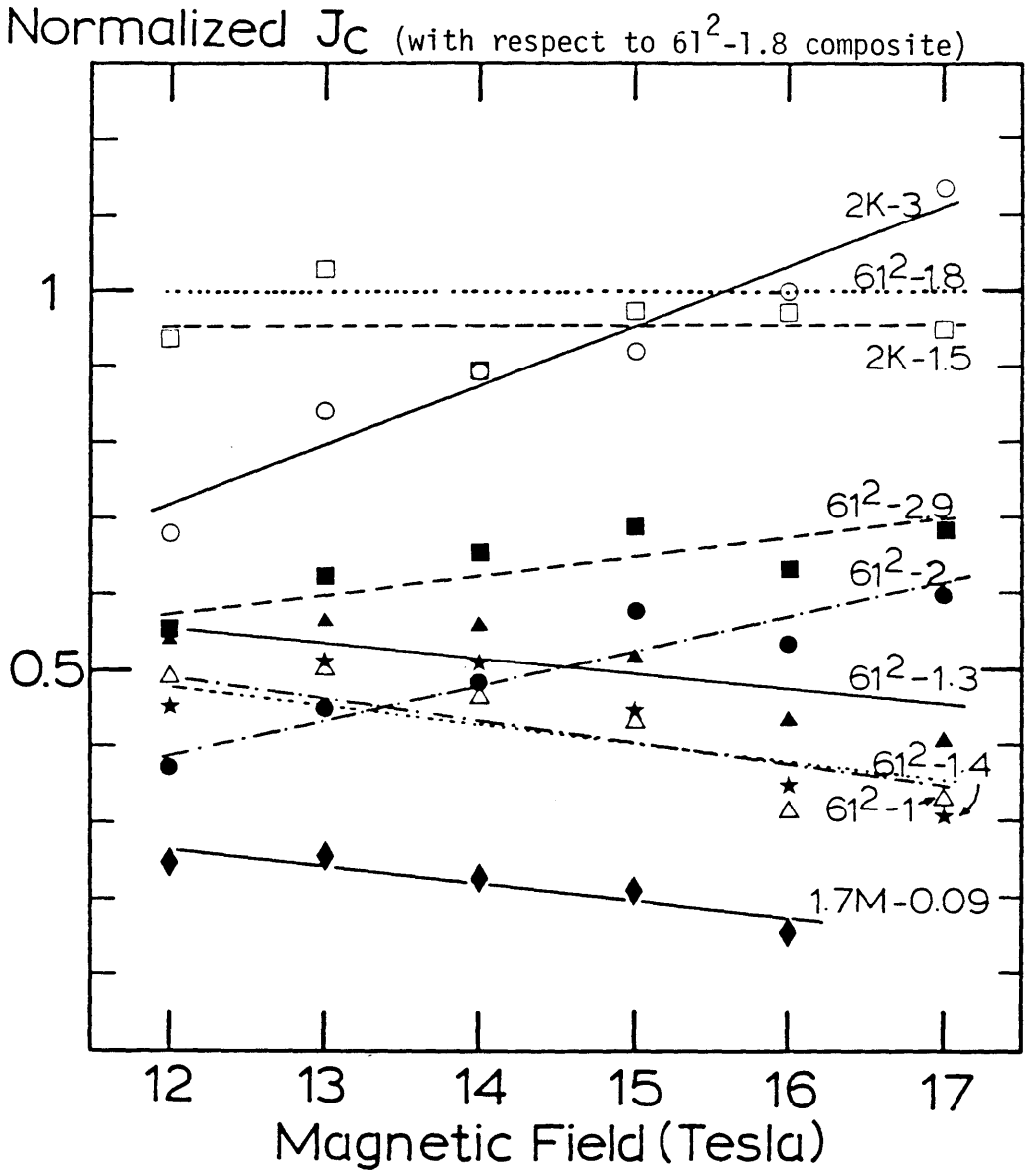

Fig. 4.1.2 Critical current density normalized with respect to the 61^2-1.8 composite. The slopes of the lines are positive for composites having filament diameters larger than 1.8um but negative for composites having smaller filament diameters.

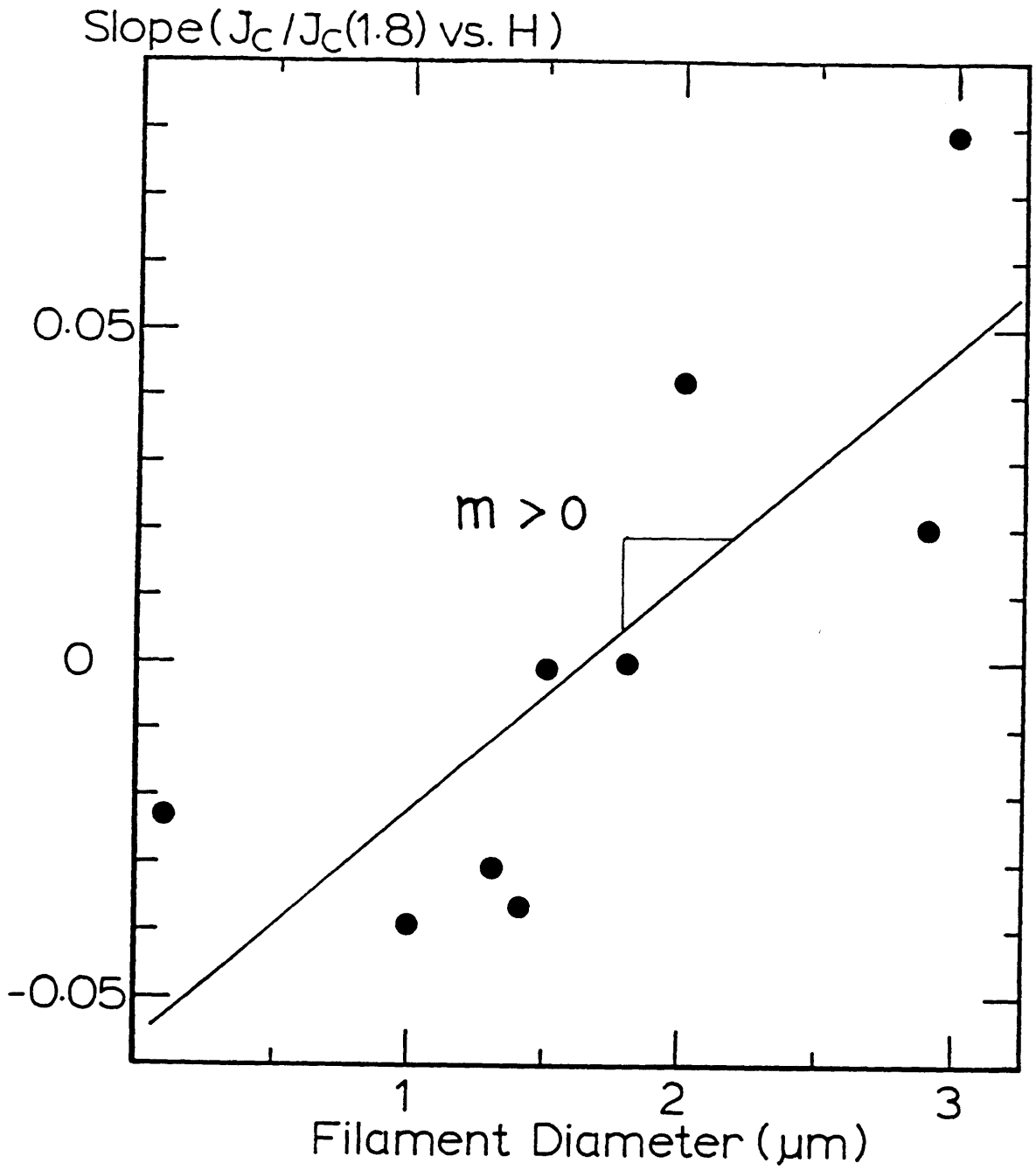

Fig. 4.1.3 Slopes of lines in Fig. 4.1.2 (normalized J_c vs. magnetic field) versus filament diameter. The slope increases as the filament diameter increases. It implies that the critical current density in high field improves as the filament diameter increases.

4.2 Flux pinning force density(F_p) and upper critical field(H_{c2})

In this section, the effort will be directed at the determination of the upper critical field (H_{c2}) of each composite from the J_c data. A relationship between H_{c2} and the filament diameter will also be sought.

According to Kramer's model (Appendix I), the flux pinning force density ($F_p = J_c \times H$), which is the maximum resistance of a material to the deformation of the flux line lattice (FLL) subjected to the Lorentz force ($F_L = J \times H$), for the high field region can be expressed as

$$F_p = J_c \times H = C_s H^{1/2}(H_{c2}-H)^2 \qquad (1)$$

where J_c is the critical current density in the applied magnetic field H, C_s is an appropriate constant for the superconductor, and H_{c2} is the upper critical field of the material.

Researchers frequently use a modified form of Kramer's equation as

$$(J_c H^{1/2})^{1/2} = C_s{}^{1/2}(H_{c2}-H) \qquad (2)$$

to check whether the data fits to the model. If a superconductor follows Kramer's rule, then the data should fit to a straight line in a $J_c{}^{1/2}H^{1/4}$ versus H plot. The upper critical field can be found as the intercept on H axis.

The experimental data were modified to be used for equation (2) and plotted in Fig. 4.2.1. The curves are not straight lines and deviate from the prediction by the model. Rather all curves have a unanimous trend of bending upward in the very high field region. It was doubtful whether the value of H_{c2} obtained from this equation would be appropriate for these superconductors. Furthermore, there have been frequent reports on this type of deviation [23,24]. Even though Kramer's model does predict the overall trend quite well, a slight

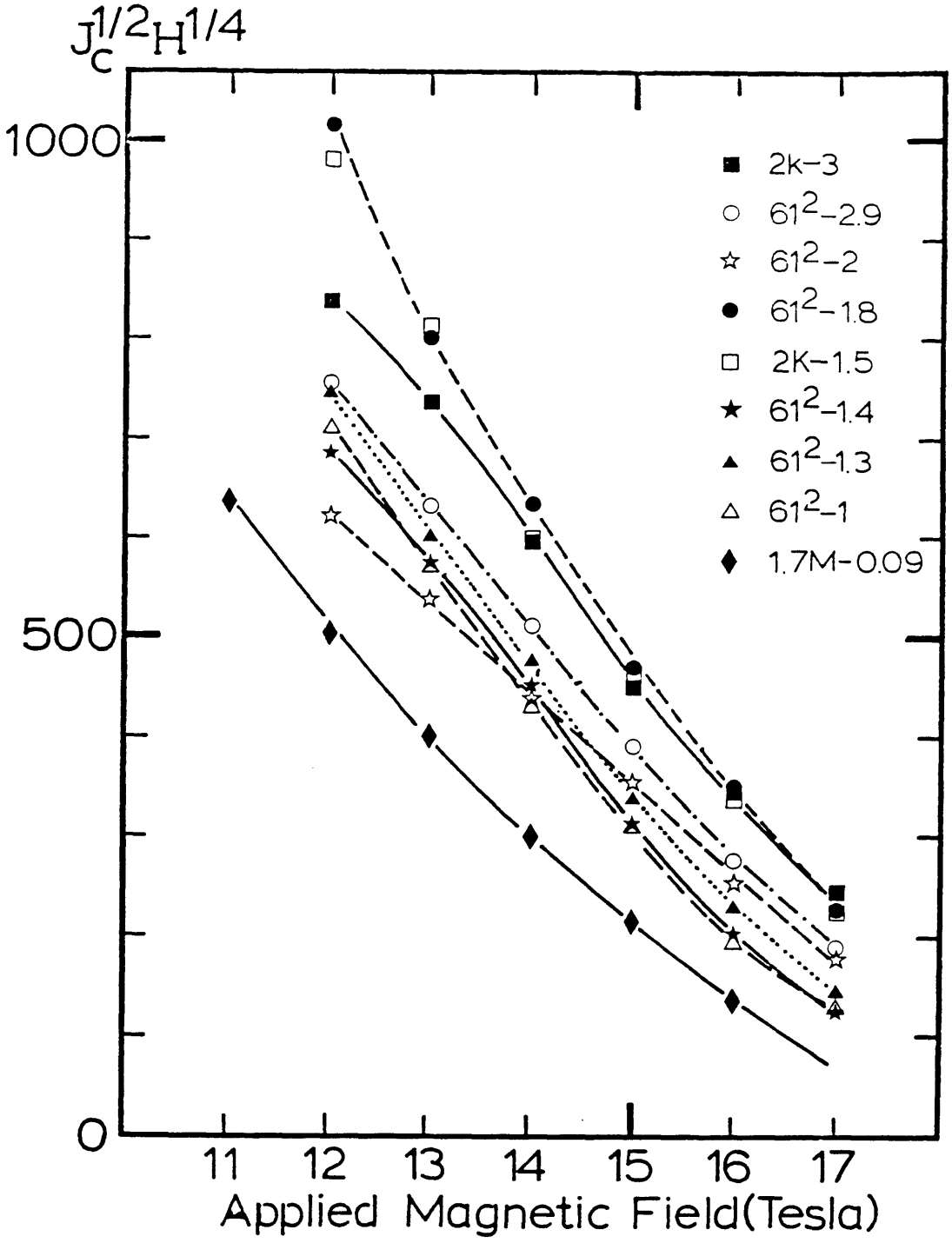

Fig. 4.2.1 Kramer's function ($J_c^{1/2}H^{1/4}$) of various composites. The curves are not straight lines and deviate from the prediction of the Kramer's model.

modification can better describe the aforementioned behavior.

Such a modification was attempted (Appendix I), assuming that the shear modulus of the flux line lattice could be expressed in terms of the power of $(H_{c2}-H)$ as in Kramer's expression but with a variable power index. The flux pinning force density for high field region then can be written as

$$F_p = J_c H = K_s H^{1/2}(H_{c2}-H)^n \qquad (3)$$

where K_s and n are the appropriate constants for a superconductor. By trial-and-error, the value of n was decided as 3, which seemed to fit for most composites, instead of 2. Once the value of n was fixed as 3, it was possible to find out the upper critical fields (H_{c2}) as the intercept on H-axis in the $(J_c H^{1/2})^{1/3}$ versus H plot.

Using the data in Table 4.1.2, the H_{c2}'s of those superconductors were determined and listed in Table 4.2.1, and plotted as a function of the filament diameter in Fig. 4.2.2. This figure shows the relationship between the H_{c2} and the filament size. There was a general trend that the upper critical field decreases as the filament size becomes smaller. An attempt to interpret this trend will be performed in the discussion (chapt. V) with the microstructural information of sections 4.3 and 4.4.

Table 4.2.1 Upper critical fields (H_{c2}'s)* of composites

Composite**	H_{c2}(Tesla)
2K-3	20.83
61^2-2.9	20.24
61^2-2	20.86
61^2-1.8	19.88
2K-1.5	19.88
61^2-1.4	19.31
61^2-1.3	19.45
61^2-1	19.19
1.7M-0.09	18.78

* Determined using the equation $J_c H = K_s H^{1/2}(H_{c2}-H)^3$ and the data in the Table 4.1.2

** The label defines the specification of a composite as follow;
(No. of filament)-(Nominal diameter of filament in μm unit)
e.g. 1.7M-0.09 composite contains i.7 million filaments of 0.09μm nominal diameter.

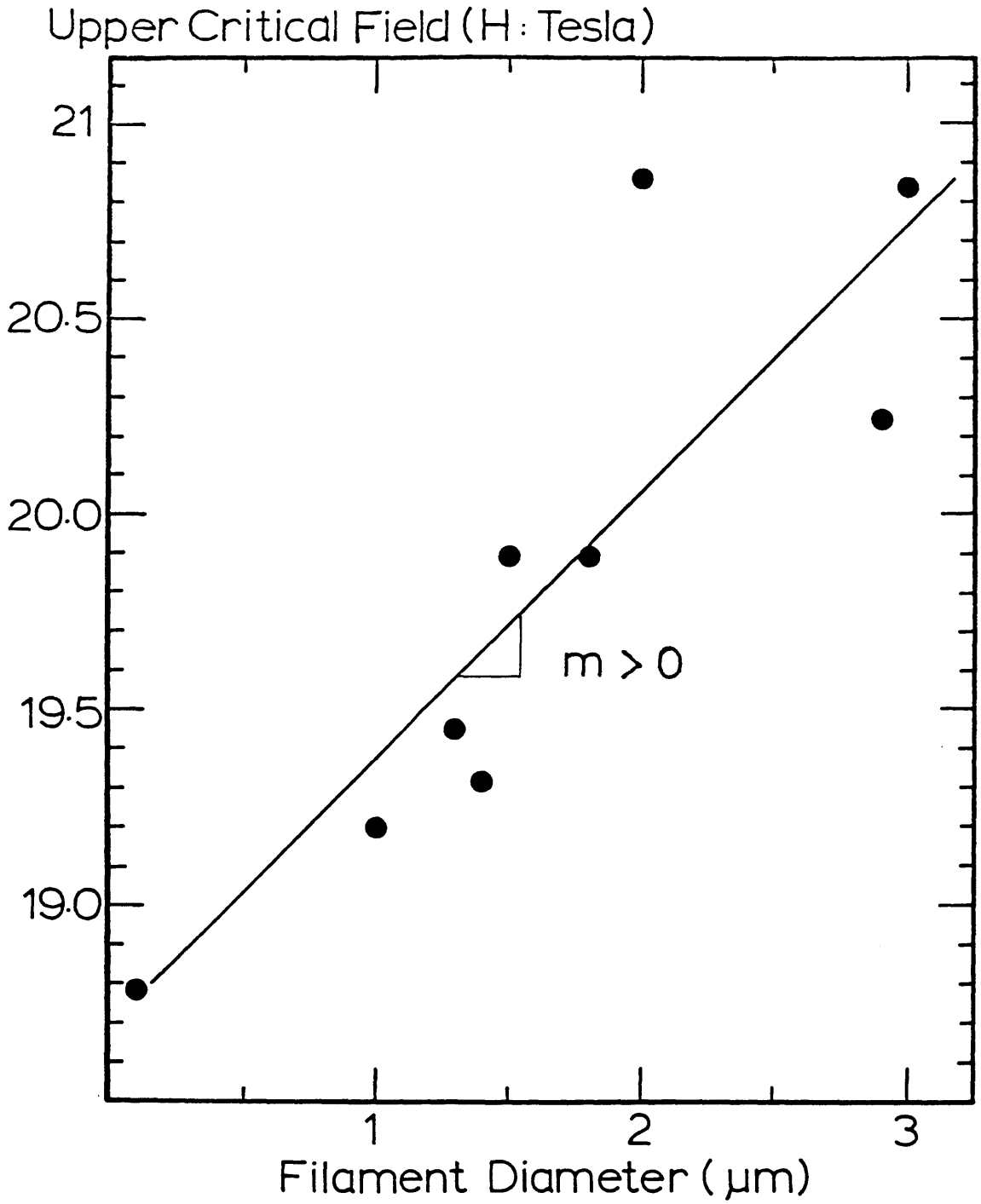

Fig. 4.2.2 Upper critical fields(H_{c2}) of various composites. Composite with larger filament diameter shows higher upper critical field.

4.3 Microstructures of the unreacted filaments

As-drawn filaments

The filaments of the as-drawn wire had highly corrugated surface with sharp ridges and valleys (Fig.4.3.1(a)). The as-drawn composites had experienced severe deformation. For instance, the smallest area reduction ratio was more than 10,000 for the 61-filament composite, and the largest was as high as $2x10^8$ for the 0.8M- and the 1.7M-filament composites. The Nb filaments, just like all other BCC crystals, had been subjected to a plane-strain condition during the plastic deformation process[25]. The observed highly corrugated surface might be attributed to the anisotropic deformation condition. This condition produced a ribbon-like filament, when the diameter was of the order of 0.1μm [26]. In the present study, due to the limit of microscopic resolution, only a fading indication of such morphology was observable.

Due to the highly irregular cross-sectional shape of filaments, measurement of filament diameter is not practical at all. Rather, the nominal diameter was calculated from the obtainable information -- such as the diameter of composite, the volume fraction and the number of filaments. Those calculated nominal values are listed in Table 2.1.

Pre-annealed filaments

As mentioned in the chapter III, the primary purpose of the pre-annealing heat treatment was to eliminate the heterogeneous nucleation sites, from which porosities might start to develop in the later stages of processing (i.e. Sn diffusion and reaction heat treatment). In the present research, the effect of the preannealing

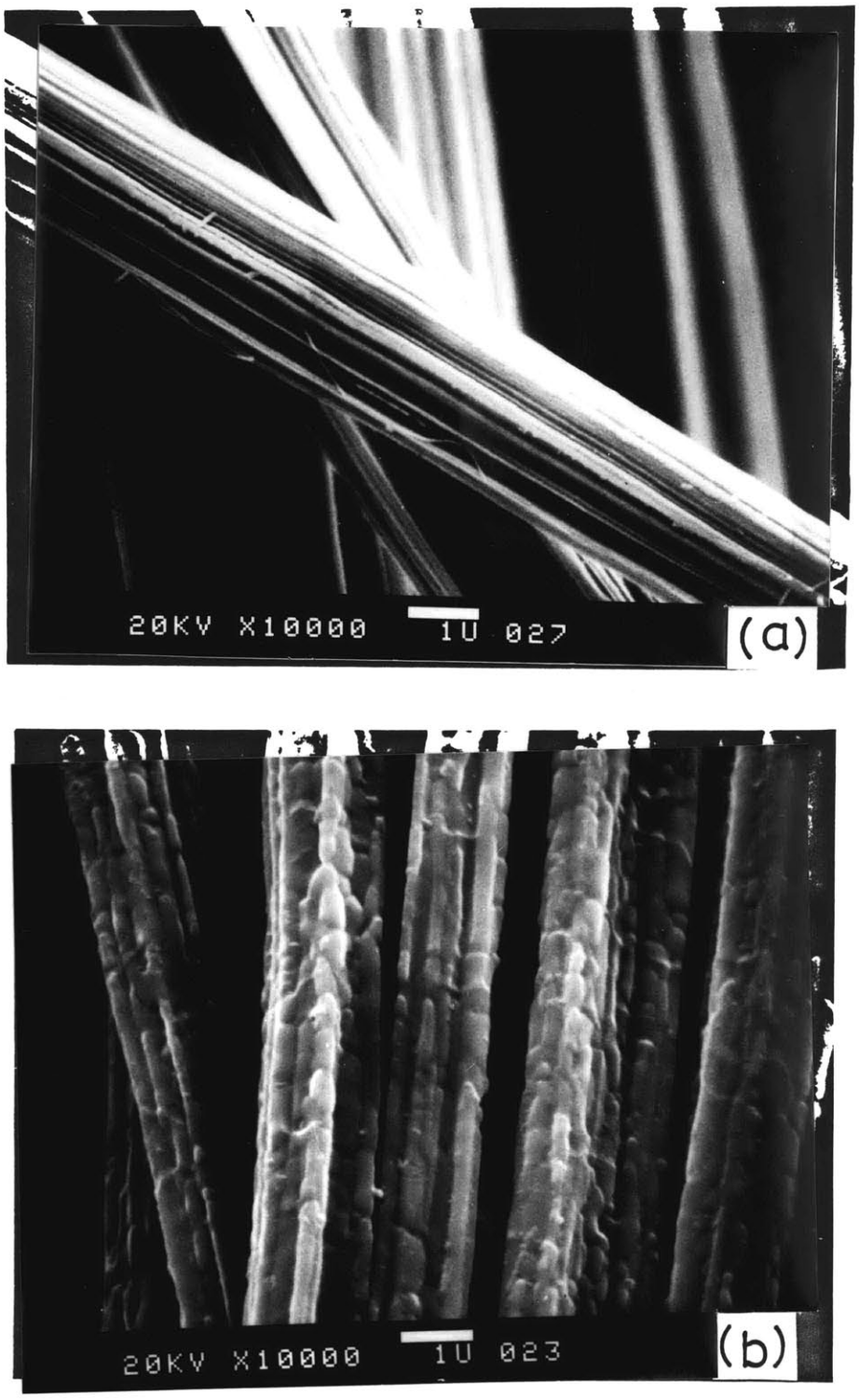

Fig. 4.3.1 Effect of the pre-annealing heat treatment on the 2um diameter filaments. (a) Highly corrugated surface of the as-drawn filament. (b) Recrystallized Nb grains cover the filament surface. Heat treated 16 hours at 650°C.

heat treatment on the morphology of filament was examined microscopically.

The preanneal heat treatment changed the sharp ridges and valleys into somewhat smoother shape (Fig.4.3.1(b)). A ridgeline transformed to a chain of Nb grains roughly cylindrical along the ridgeline. And the overall appearance of a filament was like a bundle of such chains.

The change in the ultrafine filamentary (0.8M and 1.7M) composites was remarkable. Tiny nuclei of Nb grains started to form on the filament (A in Fig.4.3.2(a)) within a few hours after the wire had been placed at 650°C. As shown in the Fig. 4.3.2(b) the nuclei had grown to the size of about 0.2μm after heat treatment for 16 hours at 650°C. The nucleation and grain growth changed the shape of a filament to a "string-of-beads". To supply the matter for the growth, some part of the filament narrowed down to a neck. In an extreme case, further development of the neck produced discontinuous filament (A in Fig. 4.3.2(b)). In a certain region where the interfilament spacing is narrow, there would be appreciable amount of mass diffusion between the adjacent filaments. Then it is quite possible for those filaments to agglomerate (B in Fig. 4.3.2(b)). The agglomeration will reduce the matrix/filament interfacial area and the energy of the system.

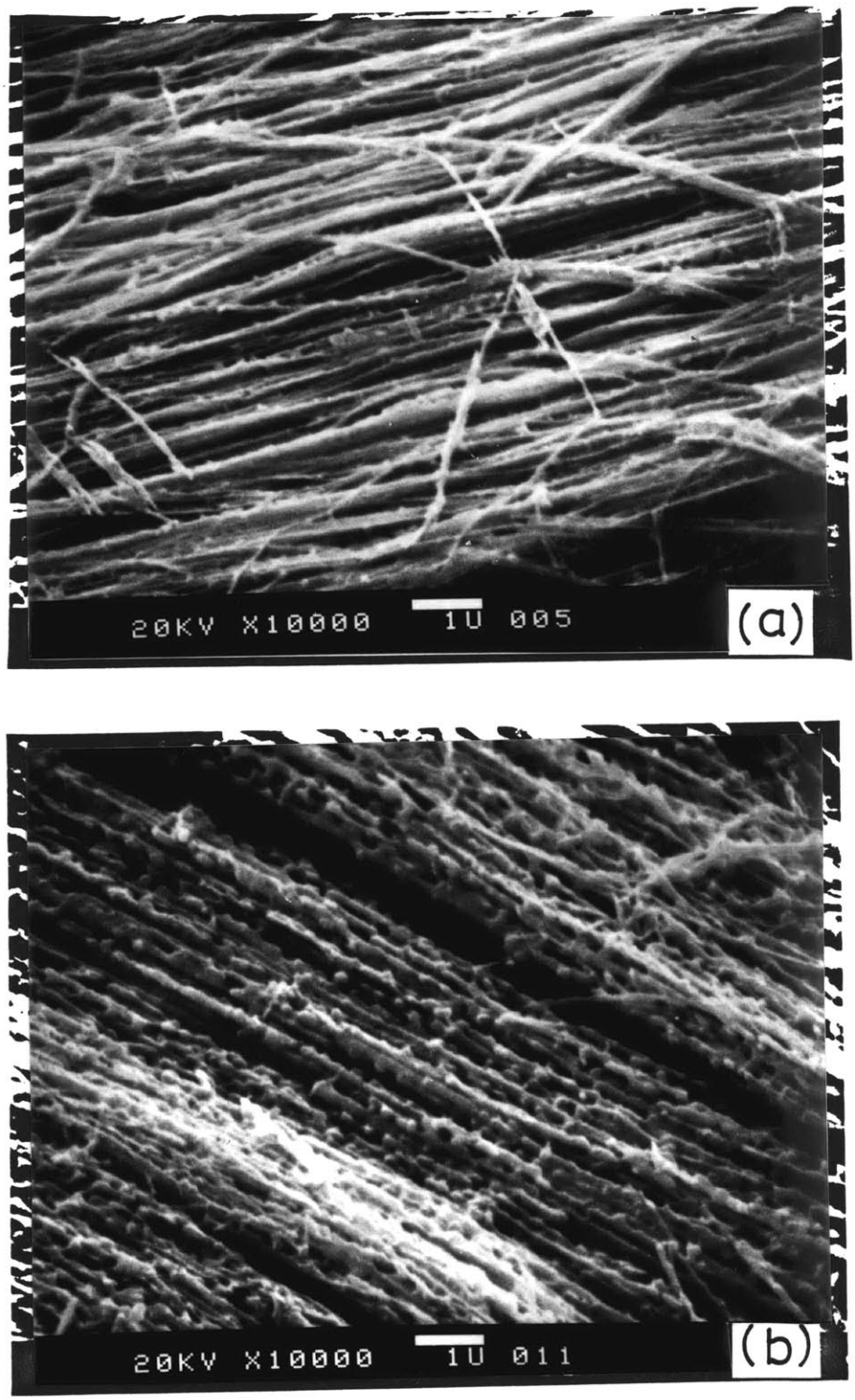

Fig. 4.3.2 Effect of the pre-annealing heat treatment on the morphology of ultrafine filament. (a) Tiny nuclei appear after 2hours at 650°C. (b) The nuclei have grown to grains of appreciable size after 16 hours at 650°C. Discontinuation(A) and agglomeration(B) of filaments are evident.

4.4 Microstructure of the superconducting phase

Columnar grains

An experiment with radioactive Sn in Nb/bronze diffusion couple [27] claimed that the major part of the Sn atoms participating in the phase growth did not come from the adjacent A15 phase layer, but from the bronze matrix. They reached a conclusion that the A15 phase grain boundary was the favored diffusion path of Sn atoms.

A TEM micrograph was taken from an area around the A15 phase growing front (Fig. 4.4.1). Part of the growing interface, which is adjacent to the A15 phase grain boundary, protruded into the unreacted Nb (A in Fig. 4.4.1). And there was a recess between the protrusions (B in Fig. 4.4.1). Behind the growing front, there were columnar grains elongated in the growing direction (C in Fig. 4.4.1). Such an appearance might be evidence that the A15 phase growth was controlled by the grain boundary diffusion of Sn atoms through the A15 phase layer.

One of the most important features of such columnar grains as a superconducting phase was the morphological (not crystallographic) orientation of the grain boundaries. The grains had grown radially. And the grain boundaries are parallel to that direction. The effect of such orientation on the superconductivity will be discussed in the chapter V. The width of the columnar grains was around 1000A.

It is worth to be noted that the concentration of Sn in the columnar grain layer is lower than the stoichiometric Nb_3Sn. The growing A15 grains are in equilibrium with the Nb terminal solution. Then the columnar layer, just behind the growing interface, would have

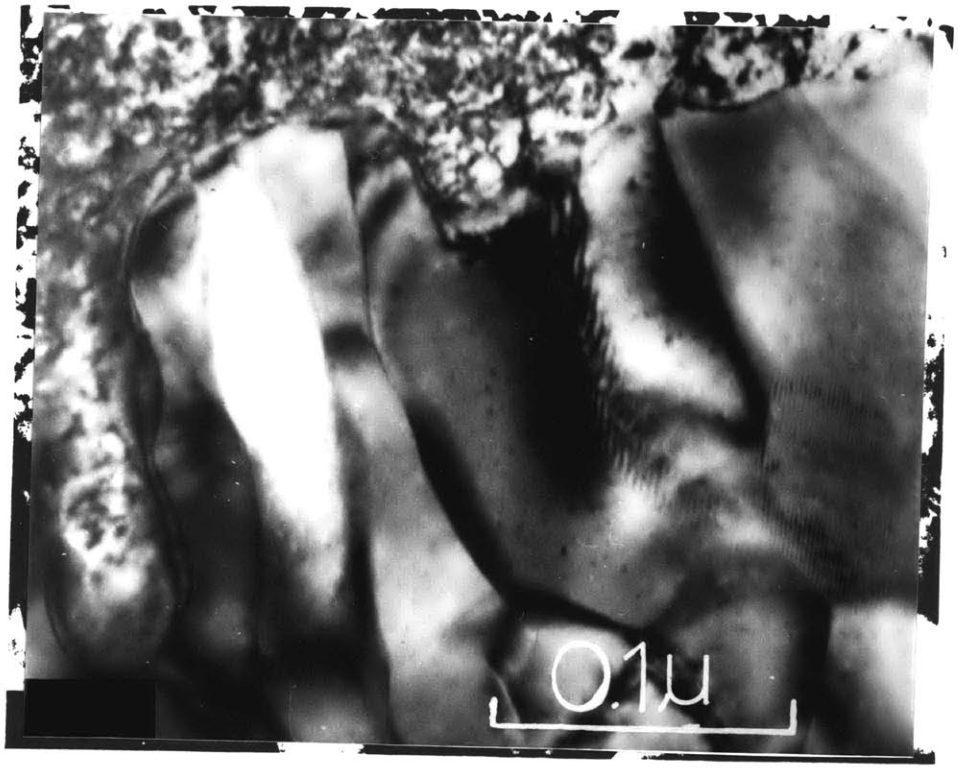

Fig. 4.4.1 A TEM micrograph shows the bronze/A15 interface. The A15 phase grows in columnar grains(C). Width of the columnar grain is less than 1000A.

the equilibrium concentration (i.e. 18 atom% Sn) [28]. However, the stoichiometric composition of the A15 structure is 25 atom% Sn [29]. Then the Sn concentration should have a gradient across the superconducting A15 phase layer. Getting close to the Sn source (i.e. bronze matrix), the concentration increased toward 25 atom% [30].

Polygonization of columnar grains into equiaxed fine grains

The Sn deficient columnar grain might have large numbers of Sn-vacancies in the A15 structure[31]. Once a vacancy exists in a crystal, atoms around the vacancy relax toward the vacancy. A long range stress field appears as a result. When the A15 phase has 18 atom% Sn, the amount of vacancy is 28% of the Sn atomic sites assigned by the A15 structure. Then the grains would have high internal stresses with distorted crystal structures. The structure should be rearranged when it admits more Sn atoms in a later stage of the reaction.

As the reaction heat treatment proceeds, more Sn atoms diffuse into the columnar grains to fill the vacancies. Then the composition of those grains approaches the ideal stoichiometry of Nb_3Sn as the reaction proceeds. The crystal structure also changes toward the perfect A15 structure. The rearrangement is accompanied by volume changes due to the substitution of vacancies with Sn atoms. However the volume change is restrictive due to the surrounding A15 phase grains. The stress field becomes to intensify and localize. Then the grains relieve the stress by nucleating and/or integrating the dislocations to polygonize into fine grains (A in Fig. 4.4.2 and 4.4.3). As a result of the polygonization and decomposition of the columnar grains, a layer of

Fig. 4.4.2 A TEM micrograph shows the area of equiaxed fine grains. Dislocations are aligned (A) to make fine grains through poligonization.

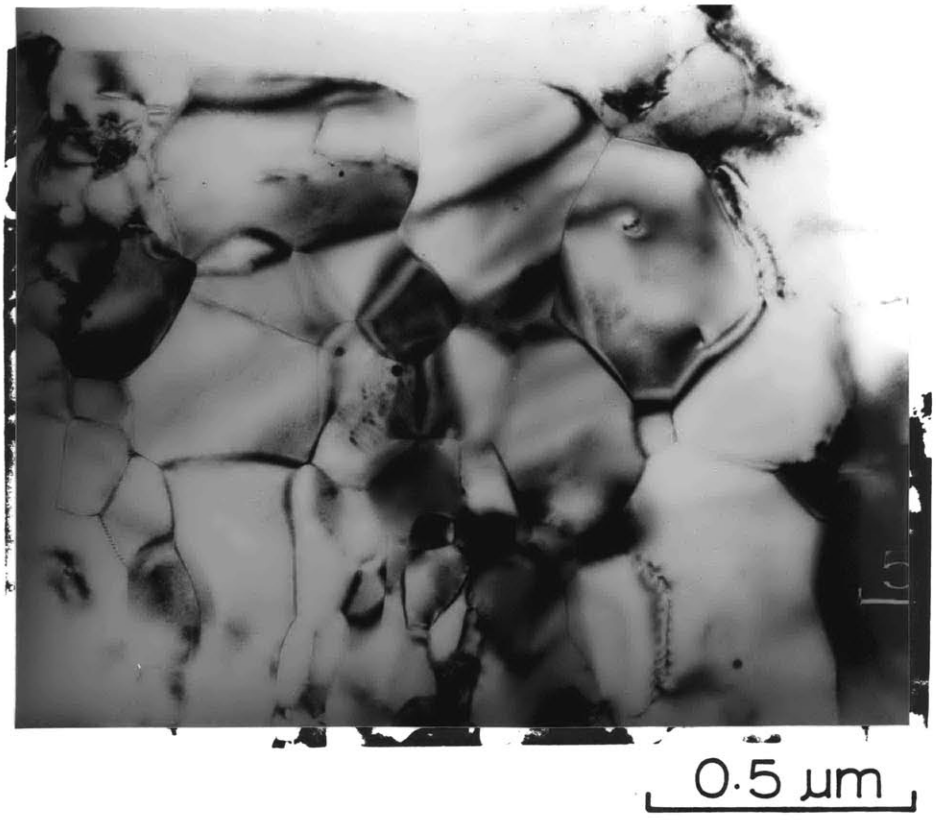

Fig. 4.4.3 A TEM micrograph of the A15 phase near the bronze matrix. One or two layers of coarse grains at the matrix/filament interface. Alignment of dislocations (A) is observable.

equiaxed fine grains exists behind the columnar grain layer [32-34] (Fig.4.4.2, 4.4.3). The diameter of the equiaxed fine grains was comparable to the width of the columnar grains (i.e. around 1000A).

Equiaxed coarse grains

Behind the equiaxed fine grains and at the A15/bronze interface, there was a layer consisting of one or two layers of coarse equiaxed grains (Fig. 4.4.3)[32-34]. The grain diameter was 0.3μm-0.5μm. The anomalous grain growth behavior is not well understood yet. However, the composition of this layer was more than the stoichiometric composition of 25 atom% Sn [32].

4.5 Microstructures of the reacted filaments

Filaments with initial nominal diameters of 1μm-3μm

The transmission electron microscopy of these filaments has been already discussed in the section 4.4. A SEM micrograph was taken from the surfaces of reacted filaments (Fig. 4.5.1). The surface was covered by coarse grains of about 0.3μm-0.5μm diameter as discussed in the section 4.4. The grain size of the layer was almost constant regardless the filament diameter.

A series of scanning electron micrographs in Fig. 4.5.2 show the cross-sectional appearances of various diameter filaments. In the 3μm and the 2μm diameter filaments (Fig. 4.5.2 (a)(b)), a large portion of core area consisted of columnar grains oriented in the radial direction (A in the figures). For the given heat treatment on those composites, the area decreased as the filament diameter decreased. Those grains almost disappeared in the filaments with initial nominal diameter of smaller than 1.8μm (Fig. 4.5.2 (c)(d)).

Ultrafine Filaments

As discussed in the section 4.3, the ultrafine filaments spheroidized and agglomerated even under the pre-annealing heat treatment. The shape instability was more severe after the reaction heat treatment. The 1.7M-0.09 composite was treated by the preannealing heat treatment at 860°C for 1 hour plus the reaction heat treatment at 600°C for 375 hours. The SEM micrographs of this material (Fig. 4.5.3) clearly showed the phenomena of spheroidization and agglomeration. Since the local volume fraction of filament was very high (about 44%),

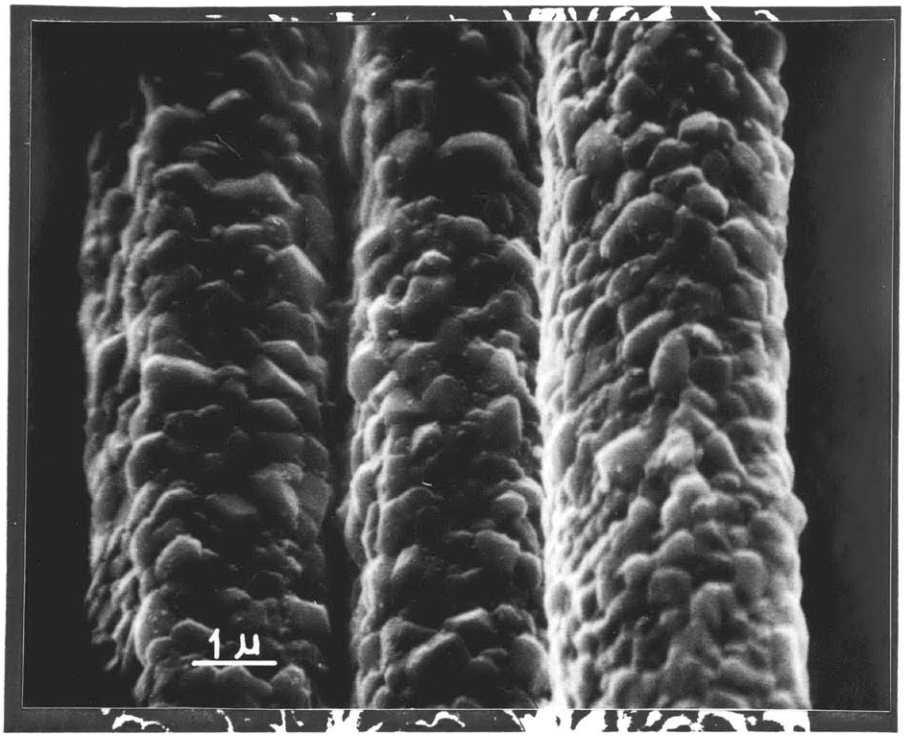

Fig. 4.5.1. A SEM micrograph of the reacted 3um diameter filaments. Reaction heat treated for 196 hours at 650°C plus 22 hours at 750°C. The entire surface of the filament is consist of the coarse grain.

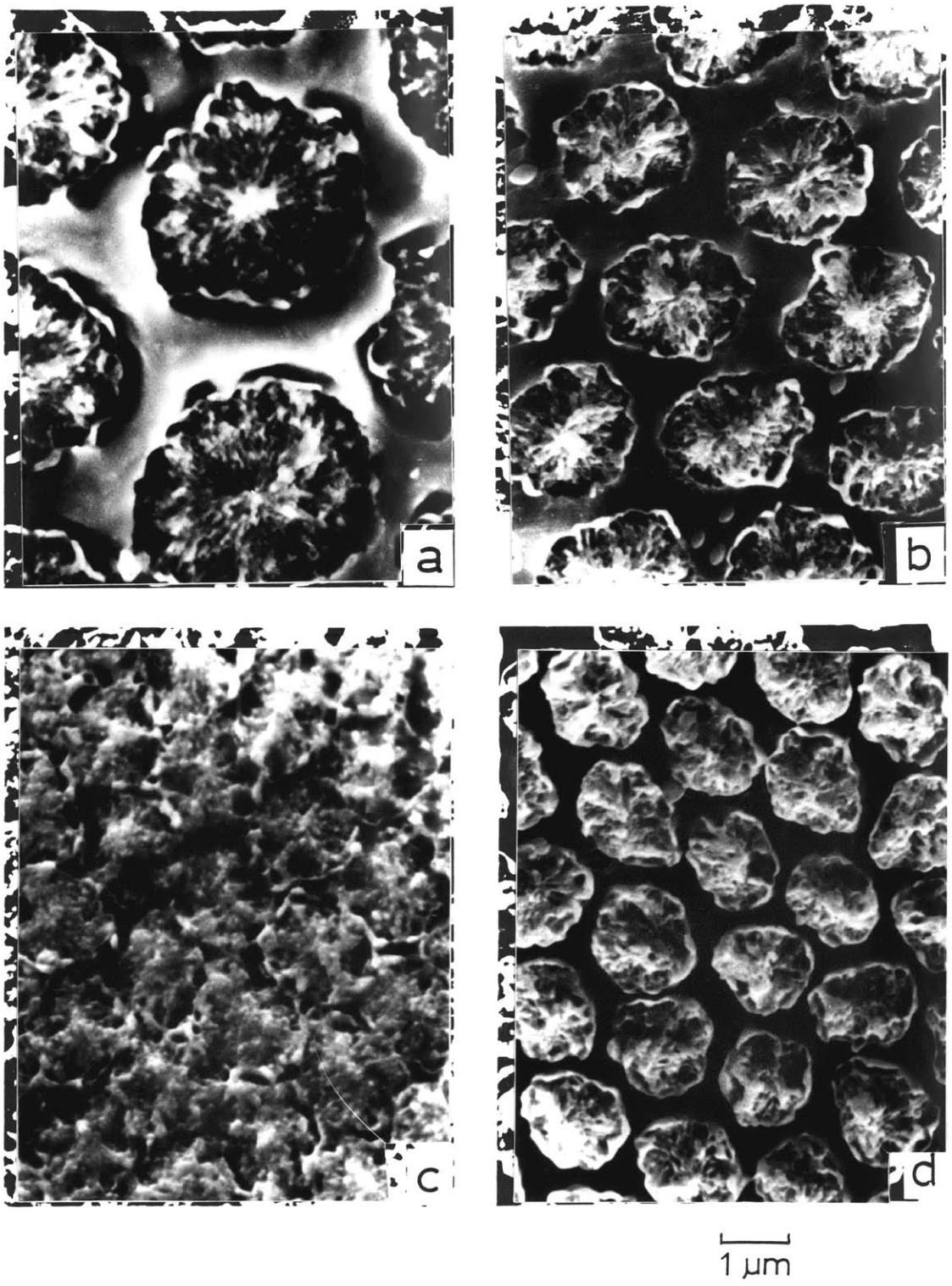

Fig. 4.5.2 Cross-sections of reacted filaments having various diameter. SEM micrographs. (a) dia.=3um,(b) 2um, (c) 1.8um, (d) 1.5um. The area of the columnar grains(A) decreases as the filament diameter decreases.

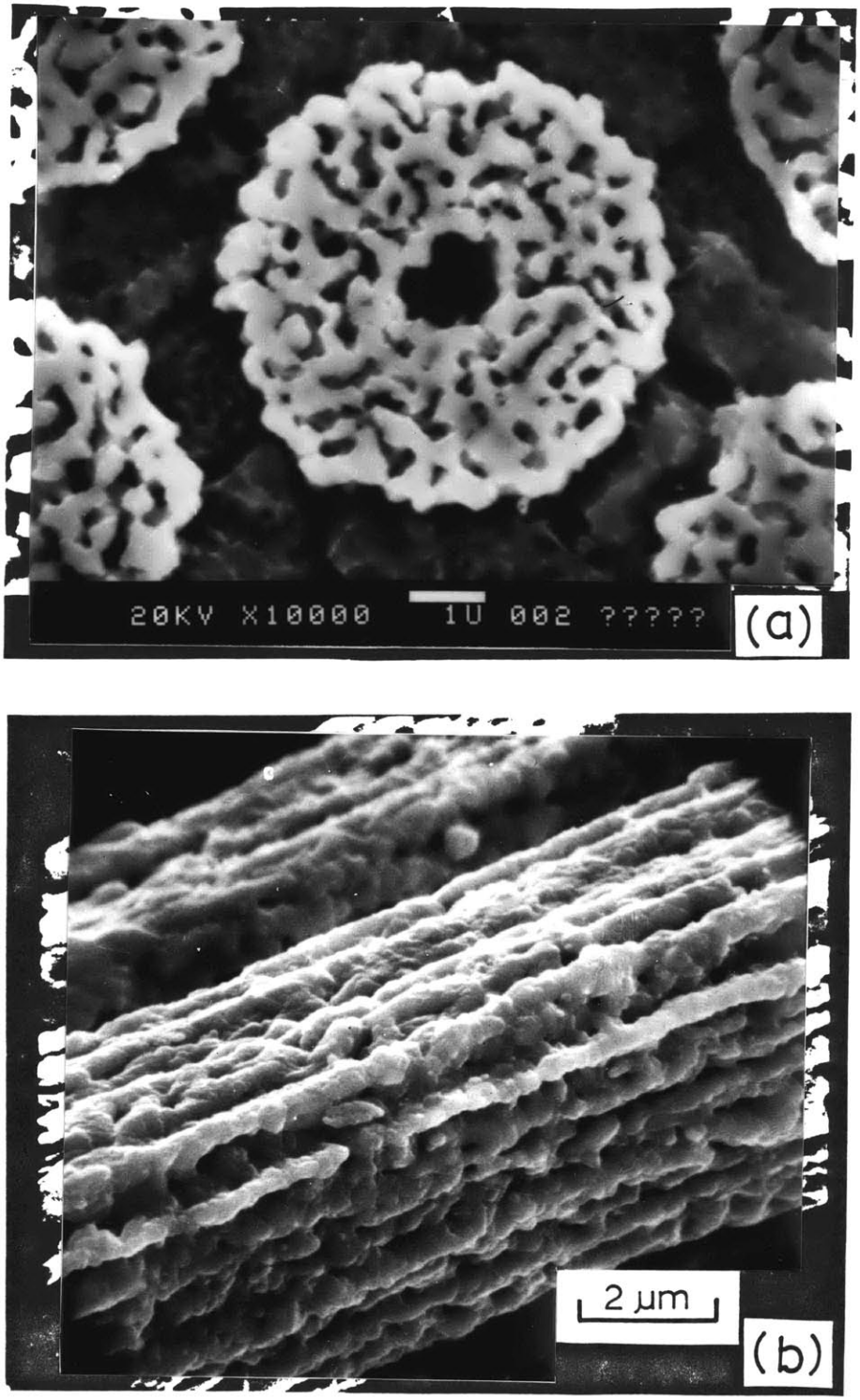

Fig. 4.5.3 SEM micrographs of the 1.7M-0.09 reacted composite. The matrix was etched out. Original geometry of the colony (Fig. 2.1(B)) has changed to completely different multiply connected A15 phase. (a) cross-section, (b) longitudinal.

the interfilament spacing was quite narrow. Then the agglomeration behavior prevailed over the spheroidization. As a consequence,the original geometry of filaments, which is shown in the Fig. 2.1(b), disappeared completely. And an entirely different morphology of multiply connected A15 phase network took over the colony of filaments. It was almost impossible to identify a single filament in this reacted composite.

The trend was also true in the 0.8M-0.1 material, which was treated with preannealing at 650°C for 16 hours plus the reaction heat treatment at 750°C for 200 hours (Fig. 4.5.4). The local volume fraction of filament in this composite was almost the same as the overall volume fraction (about 25%), which was much smaller than the previous 1.7M-0.09 wire. The agglomeration between the adjacent filaments was less probable in this composite. The A15 phase in this wire then would have more chance to break up into isolated granules with poor connectivity (Compare Fig. 4.5.3 a and 4.5.4).

The dependence of continuity on the volume fraction of Nb_3Sn had been also observed in a vacuum deposited Nb_3Sn/Cu composite [35].

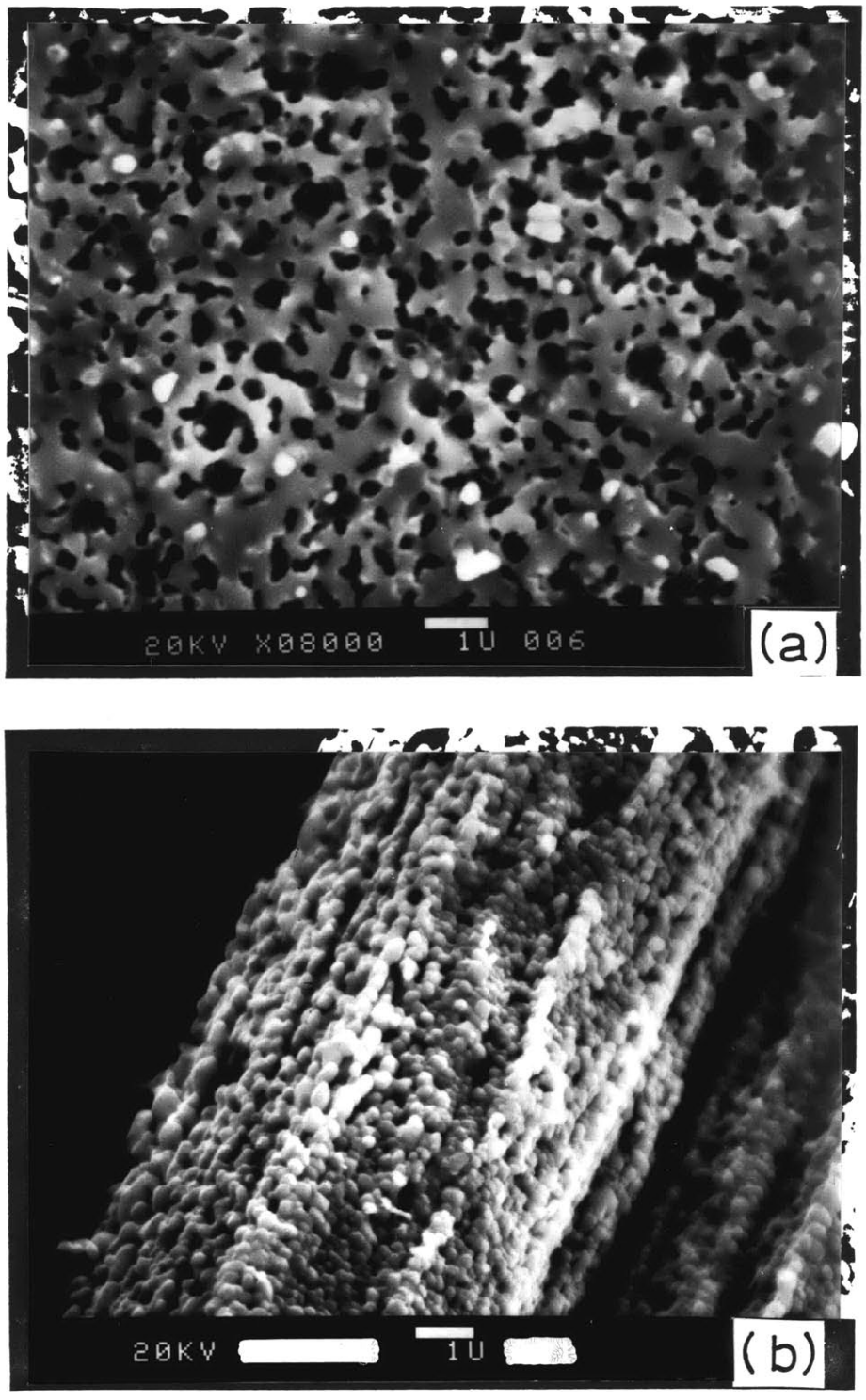

Fig. 4.5.4 SEM micrographs of the 0.8M-0.1 reacted composite. (a) A15 phase has been etched out (cross-section), (b) matrix has been etched out (longitudinal). The colony of Nb filament has been changed to the aggregate of spherical A15 grains.

V. Discussion

5.1 Optimum range of the filament size (1μm-5μm)

To find out the optimum range of filament diameter, the critical current densities of various composites have been collected from literatures (see Table 5.1.1 for the references). These values have been calibrated as the critical current densities over the filament area and tabulated in Table 5.1.1 and plotted in Fig. 5.1.1 together with the present data in Table 4.1.2. On this figure, two curves were drawn to enclose the data points in between them, and to show the general behavior of the critical current density with respect to the filament diameter. These data show that there is an optimum range in filament size at 1μm-5μm. The origin of such behavior in J_c versus filament size will be discussed below.

The lower limit

When the filament diameter was very fine, the situation turned out to be very unfavorable with only a certain possibility of supplementation. As it was revealed in section 4.5, the ultrafine filaments had severe shape instability problems in the thermally activated reaction condition. The spheroidization "breaks" the filaments to cut the current channel. The extremely spheroidized and discontinuous morphology of 0.8M-0.1 composite (Fig. 4.5.4) clearly shows the origin of the low current carrying capacity of the composite (Table 4.1.2).

The discontinuity due to the spheroidization could be supplemented to a degree through the development of agglomeration, providing an appropriate volume fraction of filament, and appropriate heat treatment schedule. The spheroids "bind" together to introduce entirely new

Table 5.1.1 Critical current densities (J_c's) over the filament area of various composites*

Filament Dia.(μm)	Vol.% Filament	J_c (unit;10^3 Amps/cm^2) 12T	14T	Heat Treatment	reference
(Conventional** External Diffusion Process)					
0.26	25	84	28	650°-200hr	21
2	25	320	140	650°-200hr	21
12	24	90	-	-	13
(Conventional** Bronze Process)					
2	22	200	120	750°-24hr	36
7	17.8	200	120	780°-168hr	37
3.5	25	162	106	740°-240hr	52
3.5	25	170	96	725°-24hr	38
3	25	170	102	-	39
2	25	228	118	-	39
1.5	25	188	102	-	39
5.1	20	117	54	700°-64hr	40
4	26.3	220	133	700°-168hr	44
(Conventional** Sn-core Process)					
0.8	18	175	56	625°-50hr	46
2	28	232	93	650°-50hr	47
17	48	17	-	-	49
26	13.8	9.4	-	-	49
34	48	7.6	-	-	49
42	18.33	7.2	-	-	49
55	19.26	2.8	-	-	49

(continued)

Table 5.1.1 (continued)

Filament Dia.(μm)	Vol. % Filament	J_c (unit;10^3 Amps/cm^2) 12T	14T	Heat Treatment	reference
(Conventional** ECN Process)					
68	26.5	99	56	675°-48hr	43
77	38	131	81	675°-48hr	43
(Modified Jelly-roll Process)					
2 x 7	25	180	84	700°-	12
(Solidification in-situ External Diffusion Process)					
0.01	23	40	10	-	41
0.1 x 2	21	115	30	550°-112hr	48
-	31.4	183		750°-24hr	50
(P/M in-situ External Diffusion Process)					
0.01	31.4	35	8	700°-24hr	42
0.13	37.5	69	21	600°-4hr	45

* Most of these data were read from the graphs in the references and calibrated for comparison.

**The term 'conventional' is used to indicate that the composite with continuous filaments is fabricated by 'tubing' and 'bundling' technique, which is different from the emerging techniques (e.g. modified jelly-roll process, in-situ process) in the sense of the wire forming.

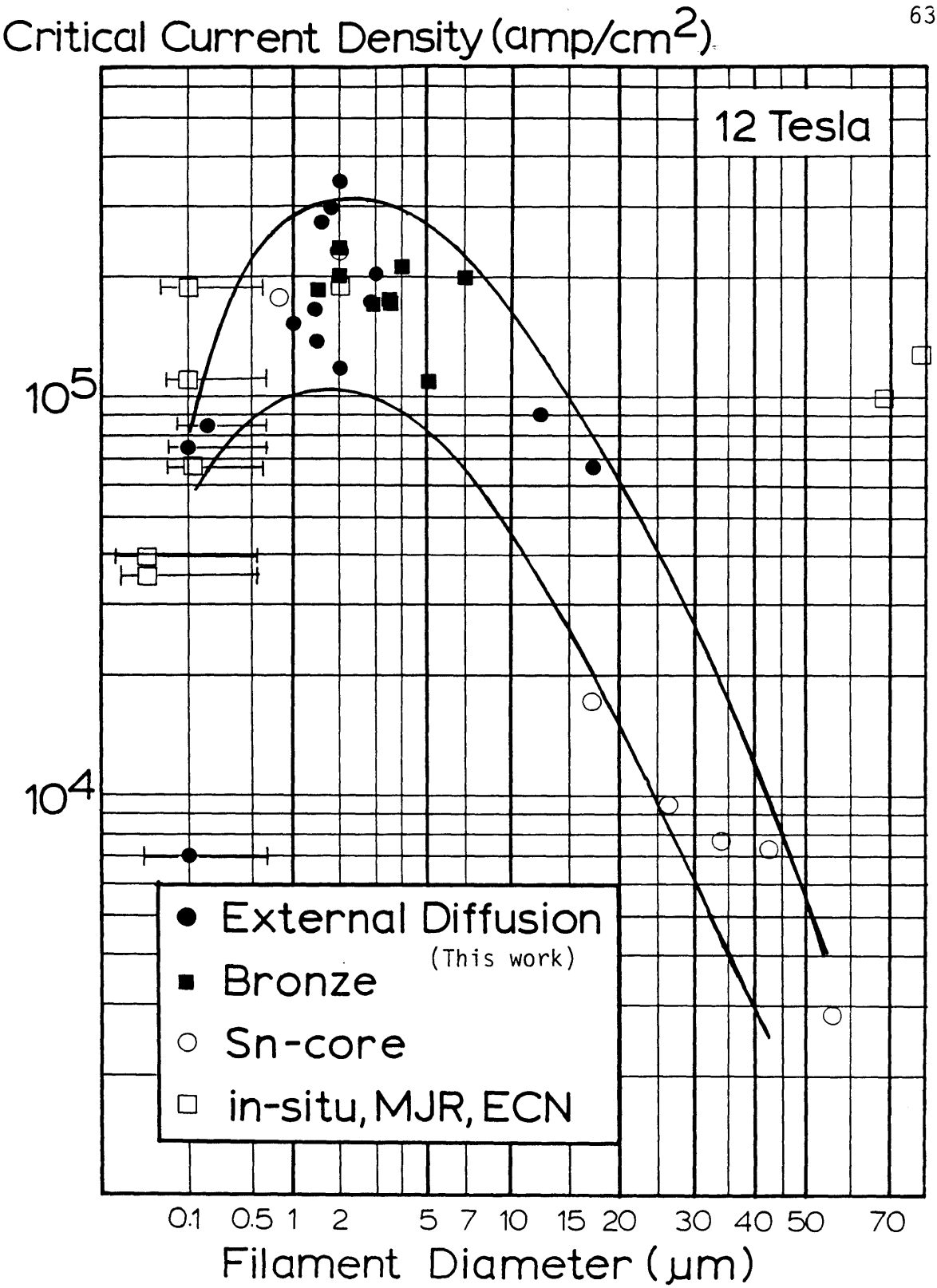

Fig. 5.1.1 Collection of the critical current densities. The numerical values are given in Table 4.1.2 (this work) and Table 5.1.1 (from literatures). Two curves enclosing the data points were drawn to show the trend of J_c vs. filament diameter. (a) 12 Tesla, (b) 14 Tesla.

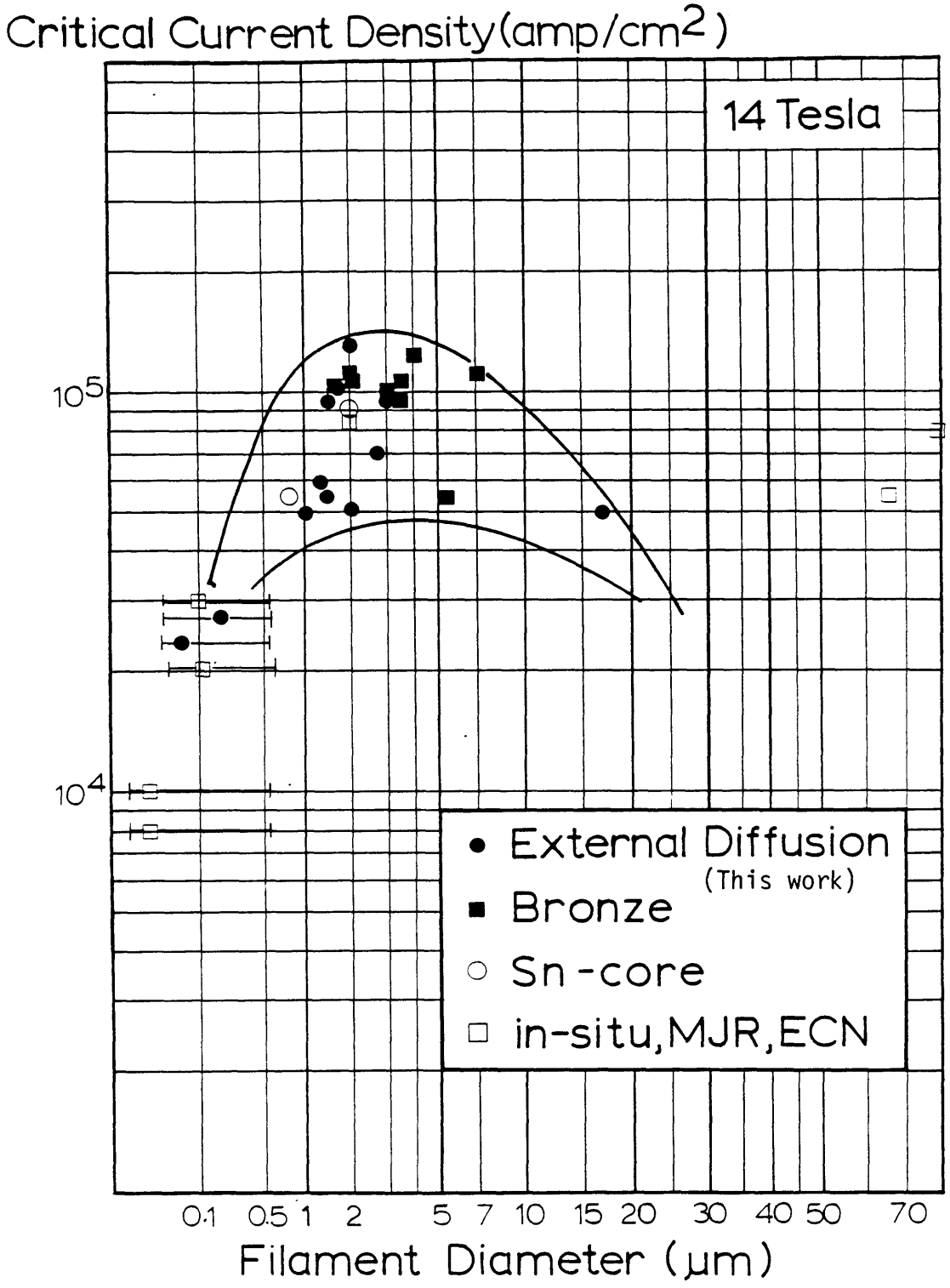

Fig. 5.1.1 (b) Collection of the critical current densities. 14 Tesla.

current channels through the formation of multiply connected superconducting phase (Fig. 4.5.3). The reasonable performance of the 1.7M-0.08 composite (Table 4.1.2) can be attributed to the recovery of the current channel through the agglomeration. Even though it was not explicitely mentioned, the spheroidization and the agglomeration behaviors were also observable in a series of in-situ composites* [26,50,51]. In the in-situ composites, the ultrafine filaments showed similar morphologies to the present 1.7M-0.08 composite.

Since the "break-and-bind" behavior made the ultrafine filamentary (including in-situ) composites work, it is not appropriate to define the filament size of those materials after the reaction heat treatment (error bars were included in the data plot of those materials in Fig. 5.1.1). Rather the local volume fraction of filament seems to be more appropriate as the comparison parameter of superconductivity. Since the critical current density is sensitive to the degree of "break-and-bind" and then to the local volume fraction of filament.

When the filament diameter is greater than the shape unstable range, the flux pinning force of the grain boundary plays a role. It is generally accepted that the grain boundary is the only one type of defect in the annealed Nb_3Sn which is effective as a flux pinnig

* The in-situ process starts with either casting a Cu-Nb melt to form a dendritic network [6,23,26,41,48, 50,51] or compacting a well-mixed Cu-Nb powder mixture [7,42,45]. The casted (or compacted) rod is then drawn down to a wire. Providing an appropriate volume fraction of Nb (>15 vol.% [17]), the originally discrete Nb forms a multiply connected fine filament after the severe mechanical deformation to a wire. Usually, the final Nb filament has a ribbon shape and the thickness of it is about 100A. Sn can be added either in the initial melt (or the powder mixture) or on the wire surface externally.

center[13]. For a given heat treatment schedule the average grain size can be assumed to be almost constant, regardless the size of filament. When the grain size is constant, a bulk material of infinite size will have the maximum grain boundary area per unit volume. If the bulk material was cut into pieces along the grain boundaries, the grain boundary area would decrease with the creation of surface. Similarly, as the filament size become smaller, the grain boundary area will decrease with the creation of the filament/matrix interface. When the filament diameter was about 13 times of the grain diameter, about 90% of the maximum grain boundary area remain as the grain boundary inside the filament (Appendix II). As the filament diameter decreases from that point, the decrease rate of the grain boundary area accelerates. For the heat treatment schedules performed on the Nb_3Sn superconducting composites to date, the grain size scatters around 1000A. Then the filament of about 1.3μm diameter has grain boundary area which is 90% of the maximum. Consequently, filament diameters less than about 1μm seem to be unfavorable for the flux pinning force of the composites.

The upper limit

On the other hand, when the filament size becomes larger, the heat treatment schedule and the filament geometry limit the volume of the superconducting phase and the grain boundary area. Usually, Sn atoms diffuse into the reaction area from the outside of a filament. Then, due to the diffusion-assisted process of the superconducting phase formation, a large filament needs a long time heat treatment to convert

all its content into the superconducting phase. When the reaction heat treatment time is short for the complete conversion of the filament to Nb_3Sn, there remains unreacted Nb core. It has the effect of reducing the volume fraction of the superconducting phase. However, employing a long reaction heat treatment time for the complete conversion, the grain size will increase to reduce the grain boundary area. There should be a compromise between the volume of superconducting phase and the grain size. Fortunately, through an appropriate choice of the filament diameter, one might select a heat treatment schedule which does convert all the content of the filament without significantly increasing the grain size.

There is much evidence that bronze processed filaments with larger than about 3.5μm had unreacted Nb cores [32,52,53,54]. That is probably due to the small amount of Sn in the initial bronze matrix*. However in the external diffusion process, one might apply large amounts of Sn insofar as the processing problems (i.e. beading, delamination, etc.) can be avoided during the heat treatment stage. Thus a larger diameter filament could be completely reacted. However, the author believes that the maximum diameter should not exceed about 5μm to minimize the volume fraction of the columnar grains from the discussion in the following section.

---

* The initial Sn concentration in the bronze matrix is limited by the maximum solubility of in the terminal solution. Assuming that all of the Sn in the initially saturated matrix can participate in the formation of Nb_3Sn, the volume of the filament should not exceed 25% for the complete converson.

5.2 The characteristics of each of the three morphologies

It has been observed (section 4.4) and reported [32-34] that the Nb_3Sn layer in a filament consisted of three concentric shells with different morphology and concentration (Fig. 5.2.1) ; The growing front had columnar grains oriented toward the growing direction. Those grains had lower Sn concentration than the stoichiometric Nb_3Sn. Behind the columnar layer, there are equiaxed fine grains with almost exact stoichiometric composition. And the outermost shell consisted of several layers of equiaxed coarse grains. The coarse grains had higher Sn concentration than the stoichiometry.

Characteristics of the columnar grains

The role of the columnar grains can be understood with the flux pinning mechanism of the grain boundary.

The origin of the flux pinning force is the interaction between the core of fluxoid and the defect, both in the "imperfect" superconducting state [2]. In type II superconductors (e.g. Nb_3Sn), the magnetic field penetrates the material to minimize the energy of the system when the applied field exceeds the lower critical field (H_{c1}) of the superconductor. Inside the superconductor, the penetrating magnetic field decomposes into fluxoids which have normal state cores. There is a strong tendency for the fluxoid to be pinned at a defect which is also in the normal state.

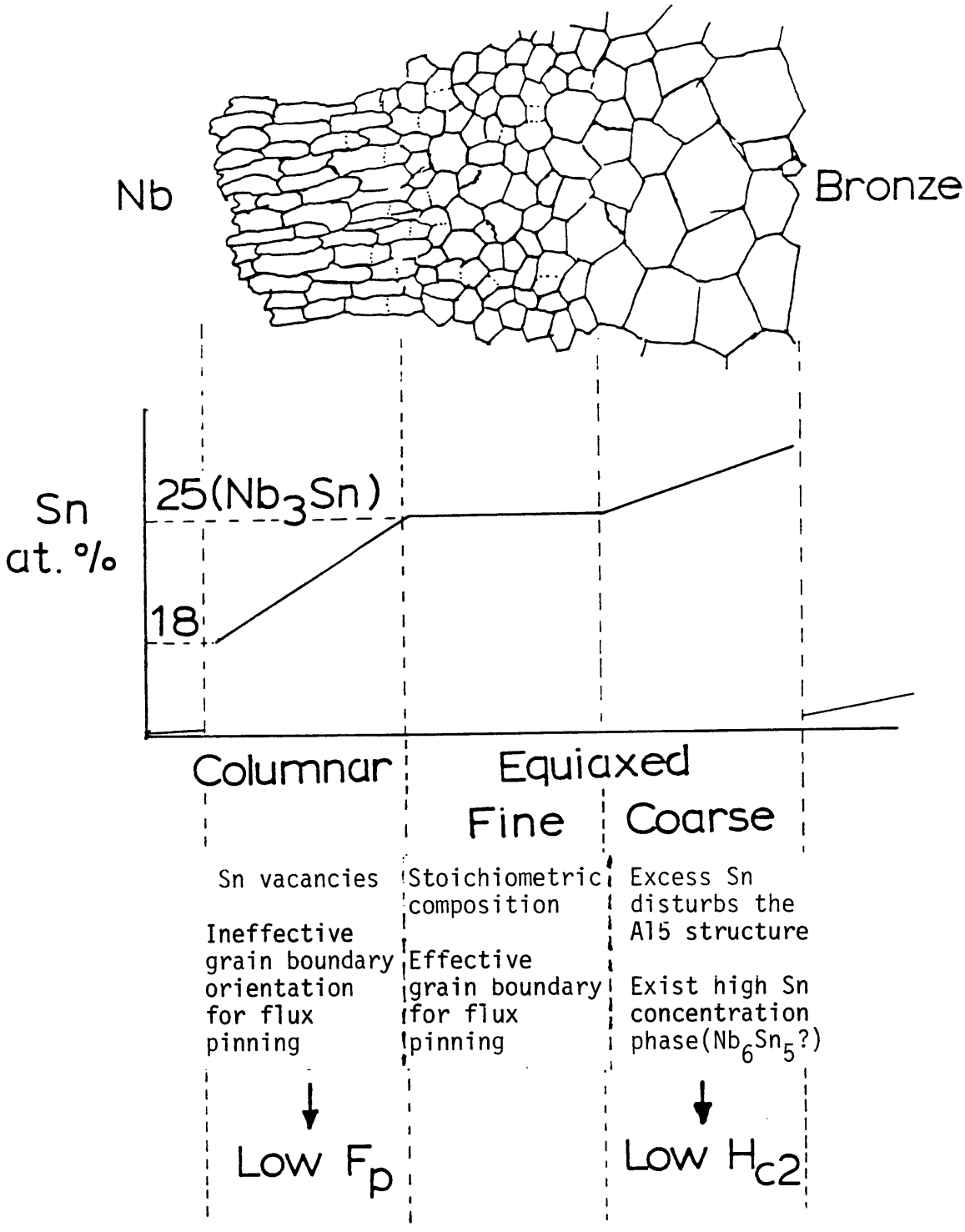

Fig. 5.2.1 A schematic illustration of the morphologies, the concentration profile and the properties of the A15 layer.

Since the grain boundary is a planar defect, the grain boundary acts as a potential valley. When the grain boundary is a "normal"* boundary, the fluxoid feels deep potential well moving across the boundary [55]. But there would be negligible potential difference, when the flux moves along the boundary (i.e. "parallel" boundary). As a result, the "normal" grain boundary is a strong pinning center. But the boundary changes to a weak pinning center, when it becomes a "parallel" boundary.

The columnar grains were oriented in radial direction. And the density of "parallel" grain boundary in the columnar structure is higher than that in the equiaxed fine grains layer. Then the density of strong pinning center in the columnar grains layer is lower than that in the equiaxed fine grains layer. The larger the areal fraction of columnar grains layer is, the lower the flux pinning force density will be. And the characteristics of the flux pinning centers seem to be particularly important in the low fields, because the Lorentz force is very high in such fields.

The composites with large diameter filaments(2K-3, 61^2-2.8) showed relatively low critical current densities in the low magnetic field regime of the present research compare to the high field performance (Fig. 4.1.2). This trend might be attributed to the large areal fraction of the columnar grain boundary in those composites (Fig. 4.5.2(a)).

---

* For the sake of brevity, when the direction of the fluxoid movement (i.e. the direction of the Lorentz force) is normal to the tangential plane of a grain boundary, it will be named the "normal" boundary. When it is parallel, the "parallel" boundary.

Characteristics of the coarse grains

The maximum Sn concentration of the A15 phase is 25.1 atom% [28]. However, the composition of the coarse grain layer deviated from the stoichiometry of Nb_3Sn toward the Sn-rich direction [32]. Then the excess Sn will introduce either or both of the following two situations; (i) Disturb the one-dimensional Nb chain structure of the A15 phase, (ii) Form a higher Sn concentration phase (presumabley Nb_6Sn_5). There have been several reports that the one-dimensional continuous Nb chains in A15 structure is the primary reason of the high critical temperature and the high H_{c2} in Nb_3Sn [56,57]. They further claimed that disturbance of the chain structure produced low critical temperature and H_{c2}. On the other hand, it was reported that the Nb_6Sn_5 phase has extremely low critical temperature and H_{c2}[58]. Even though it has not been confirmed which is the case, these situations will result in low H_{c2}. In a very high field close to H_{c2}, the flux penetrate the superconductor almost completely. The flux line lattice (FLL) parameter becomes very small. Assuming a triangular FLL, the parameter is 118.6A, when the magnetic induction is 17 Tesla. In such a high field, only a part of the fluxoids would be pinned at strong pinning centers. Rest of the fluxoids resist the Lorentz force through the shear modulus of the flux line lattice [60,61]. The shear modulus of a FLL is usually expressed as a power of the difference between the H_{c2} and the applied field. Then the material with lower H_{c2} will have lower shear modulus and lower J_c especially in high magnetic fields close to H_{c2}.

Furthermore, due to the large grain size, the grain boundary area

and the density of the strong pinning center in this layer is lower than that in the equiaxed fine grains layer.

Therefore the composites with large areal fraction of coarse grain, which are the small diameter filament composites (e.g. 61^2-1,61^2-1.3 etc) in this research, showed relatively low critical current densities over the fields of interest. However, the arguement on the low H_{c2} would be restricted only to the coarse grain. Then the trend of low J_c in high fields is prominent in a small diameter filament composite.

An alternative explanation for the low H_{c2} of the small diameter filament might be possible using the concept of the residual stress within the filament. There is much evidence that the H_{c2} of Nb_3Sn decreases as the stress increases[18,19]. Due to the difference in the thermal expansion coefficient between the Nb_3Sn filament and the bronze matrix, cooling down the composite from the reaction temperature produces residual compressional stress in the filament. The residual stress increases as the filament diameter decreases. Then a smaller diameter filament will produce lower H_{c2}. However, it should be remembered that, in certain situation, a colony of closely spaced fine filaments acts as a large diameter filament due to the "coupling effect." Further discussion on the residual stress effect is beyond the scope of this research.

Characteristics of the equiaxed fine grains

Out of the wires tested in this research, the 61^2-1.8 composite showed the highest critical current densities (Table 4.1.2) within the

fields of present interest. This composite had large volume of the equiaxed fine grains (Fig. 4.5.2(c)). The high J_c and H_{c2} of the composite might originate from the microstructure.

As a possible result of the polygonization (section 4.4), the diameter of the equiaxed fine grain was comparable to the width of the columnar grain. Then the fine grain layer should have the largest grain boundary area. Due to the shape of the grains, the density of "normal" boundary in this structure is larger than that in the columnar grains and no less than that in the coarse grains. Then this layer would have the highest density of strong pinning centers (i.e. the density of "normal" grain boundary area) among those three morphologies. This is favorable for low field performance.

Furthermore, the composition was almost stoichiometric, so that the continuity of Nb chain in the A15 structure seems to be well maintained Thus the fine equiaxed grains layer have high upper critical field (H_{c2}).

The layer of fine equiaxed grains have characteristics favorable for both high and low field regions within the present research. The filament of optimum size should have the largest areal fraction of the equiaxed fine grains.

Summary

The above discussion on the microstructure and the J_c relation can be schematically represented as in Fig. 5.2.2. The volume fraction of each morphology (columnar grain, equiaxed fine grain, equiaxed coarse grain) is a function of the heat treatment schedule and the filament

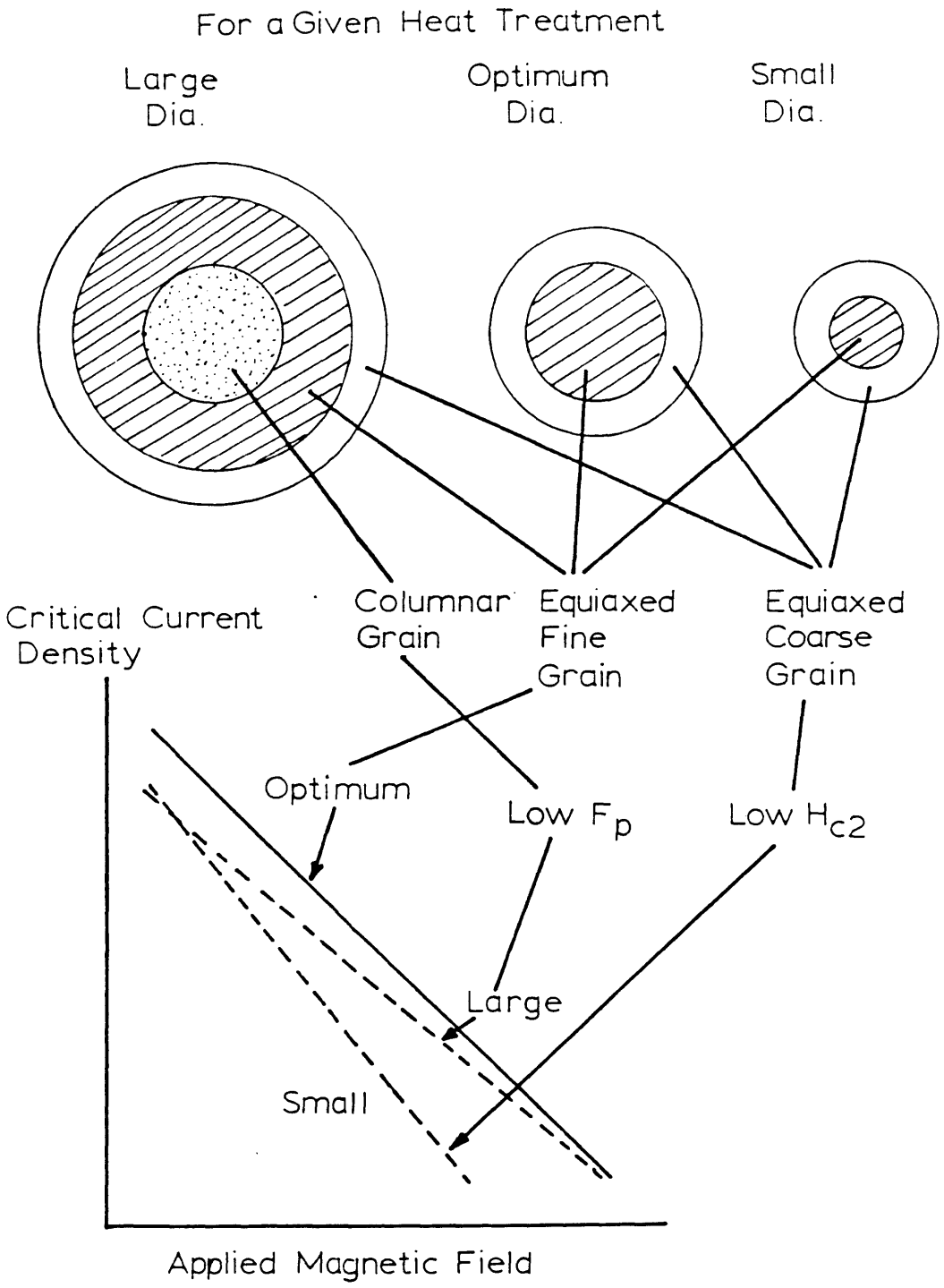

Fig. 5.2.2 Effect of the filament diameter on the critical current density vs. magnetic field behavior.

diameter. However, the thickness of the outermost coarse grains layer seems not so sensitive to the filament diameter of a composite. And it might be assumed that the thickness is almost constant regardless the diameter of a filament for a given heat treatment.

As is stated at the end of previous sub-section, the best performance composite would be the wire which has the largest volume fraction of the equiaxed fine grain for a given heat treatment. Based on the assumption in the previous paragraph (i.e. constancy of the coarse-grain-layer thickness), the largest volume fraction of the equiaxed fine grains might be obtained with the filament where the innermost columnar grains layer barely disappears for a given heat treatment. In the present research with the reaction heat treatment of 200 hours at 650°C, it happened in the filament of about 1.8μm diameter.

The volume fraction of the outermost coarse grain increases as the filament diameter decreases. And the superconductivity of the composite having smaller diameter filament than 1.8μm is largely affected by the properties of the coarse grains (i.e. low flux pinning force density and low H_{c2}). As explained previously, lowering the H_{c2} reduces the shear modulus of the FLL and the critical current density especially at high fields (Fig. 5.2.2).

When the filament diameter of a composite is greater than the "optimum" diameter (i.e. 1.8μm in this research), there is a large area of columnar grains at the core of a filament. The importance of the columnar grains increases as the filament diameter increases. As is discussed above, a typical characteristic of the columnar grains might

be the low flux pinning force density. Then the large diameter filament with large volume fraction of the columnar grain would show low flux pinning force density, which is prominent at low fields.

VI. Conclusions

To obtain a better performing superconducting composite, the effects of filament size have been studied. The size of a filament limits the microstructure of the superconducting phase and then indirectly influences the J_c through the microstructural change. After the comparison of the critical current density and the microstructure of composites with various filament size, the following conclusions could be deduced :

(1) There is a certain range of optimum filament diameter, which is roughly 1μm-5μm. When the filament diameter of a composite is smaller than the lower limit of the range, the filaments experience shape instability under the thermally activated diffusion and reaction heat treatment conditions. The ultrafine filament constructed the superconducting current network through the "break-and-bind" mechanism. Then the critical current density of the ultrafine filamentary composite is strongly dependent on the degree of the "break-and-bind", which can be controlled with the volume fraction of the filament. When the diameter is larger than the upper limit, it is hard to transform all the content of the filament into the superconducting phase with a reasonable heat treatment schedule which does not significantly increase the grain size of the A15 phase. Then the unreacted Nb core keeps the large diameter filament from exhibiting its full potential as superconducting current channel. To avoid the shape instability and the existance of unreacted Nb core, a superconducting composite should be fabricated within the filament diameter range of 1μm-5μm.

(2) Generally, the Nb_3Sn filament of diameter within the optimum range has a three concentric shell structure on its cross-section -- the outermost coarse grain shell, the columnar grains in radial direction at the core, and the equiaxed fine grains in the middle. The coarse grain has higher Sn concentration than the stoichiometric composition and exhibits low H_{c2} through a disturbance of A15 structure. And the small diameter filament, which has usually large volume fraction of coarse grain, shows low J_c at high fields. On the other hand, the filament of diameter near the upper limit of the optimum range has a large volume fraction of columnar grains at its core. Due to the predominance of the "parallel" boundary in this morphology, the flux pinning force density of the large diameter filament is low, especially at low fields.

(3) The most desirable morphology of a filament is the homogeneous equiaxed fine grains with the stoichiometric composition. This structure is almost impossible to obtain with any one of the conventional fabrication techniques. And the largest volume fraction of such grain could be obtained with the filament of diameter where the columnar grains barely disappears for a given heat treatment. The diameter was about 1.5μm-1.8μm in the present research.

VII. Future work -- suggestion of a new process

To date, most of the Nb_3Sn multifilamentary superconducting composites are made by a process, where the diffusion of Sn is unavoidable. In other word, the location of the Sn source and that of the Nb_3Sn formation are different. Scrutinizing the present research, one might notice that those problems -- formation of the columnar grains and the coarse grains, off-stoichiometric composition, and existence of the unreacted Nb core -- come from the very diffusional characteristic of the fabrication process. Furthermore, it is hard to control the grain size of the equiaxed fine grains employing the process available to date.

For the improvement of the superconducting property of a Nb_3Sn composite, a new diffusionless fabrication method should be developed to obtain the filament with a homogeneous structure of the fine equiaxed grains. Over the diffusionless characteristic, the new process should be easy to fabricate fine filamentary composite and to control the grain size. Then a powder metallurgical process seems to be the most appropriate one.

The author suggests a powder metallurgical process composed of three steps -- powder mixing, mechanical deformation to a composite wire, and reaction heat treatment. As the first step, a powder mixture of stoichiometric composition (i.e. Nb:Sn = 3:1 in atomic ratio) should be obtained. The mixture can be either of the pure elemental Nb and Sn or of certain compounds for easy fabrication (e.g. Nb and $NbSn_2$ [43,59]). Since it is known that the Cu acts as a catalyst in the Nb_3Sn formation, a small amount of Cu powder should be included to employ a

low reaction temperature in the later step. Then the powder mixture should be compacted to a rod shape for the next step. The second step is composed of the conventional wire forming processed as described in the chapter II of this article -- drilling holes and inserting rods on a Cu cylinder, extrusion, bundling and wire drawing. In this step, extreme care should be taken to keep the powder mixture from the formation of the superconducting phase, because the existance of Nb_3Sn will make the further mechanical deformation impossible. The last step is the reaction heat treatment. Since the Sn is already distributed homogeneously inside a filament, the diffusion of Sn is not necessary in this process. The heat treatment is necessary only to react the powder mixture to the superconducting compound and to obtain a desirable grain size of the compound. The author would like to call this process the "continuous filament P/M process" to differentiate it from the conventional in-situ P/M process with multiply connected filaments.

An illustration (Fig. 6.1) is given to compare the suggested process with two other popular processes -- bronze process, external diffusion process. The locations of Sn source are different from each other ; the periphery of a wire in the external diffusion process, the matrix in the bronze process, and the filament itself in the proposed process. And the advantages of the new process might be as follow ;

General advantages

(1) The Sn is already completely mixed with Nb before the reaction. Consequently, not only the whole filaments will convert to Nb_3Sn upon the reaction heat treatment but also all the problems

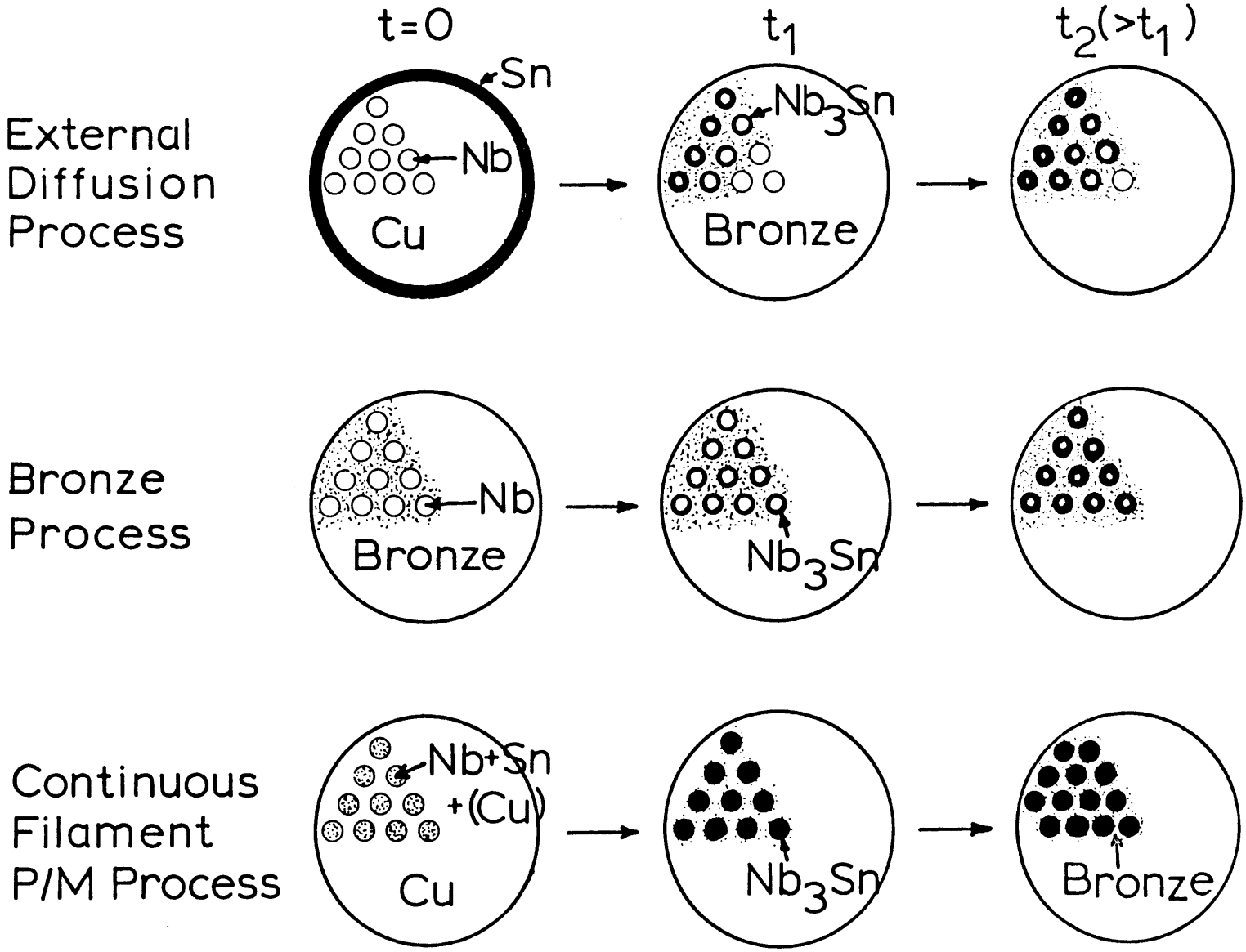

Fig. 6.1 Comparison of the superconducting Nb_3Sn composite fabrication processes

arising from the Sn diffusion (e.g. the Kirkendall porosities, inhomogeneous Sn concentration, inhomogeneous grain morphology and size) will be eliminated. And the grain size control will be very easy.

(2) The matrix is almost pure Cu which has better electrical and mechanical properties than that of the conventional bronze matrix.

Advantages over the bronze process

(1) Intermediate annealing steps will not be necessary during the mechanical deformation.

(2) The concentration of Sn can be easily controlled for the best performance of a composite.

Advantages over the external diffusion process

(1) All the problems arised from the Sn on the surface of a composite (e.g. beading, surface porosities, etc.) can be avoided.

(2) There is almost no limitation on the scale-up of the superconducting composite.

(3) The composite can be heat treated after the magnet coil construction.

Eventhough there are many advantages as above, the formation of the brittle Nb_3Sn is easier than any other process during the mechanical deformation. And the wire fabrication seems to be very difficult in this process. The immediate future work should be focused on the development of the deformation technique to overcome the difficulties. Once it is done, the following should be studied ;

(1) Find out the optimum Sn and Cu fractions of the powder mixture.

(2) Decide the heat treatment condition for the optimum grain size.

(3) Understand the relationship between the grain size and the flux pinning force.

(4) Understand the relationship between the Sn concentration and the critical current density.

(5) Decide the optimum geometry of the composite -- the diameter and the volume fraction of the filament, and the diameter of the composite.

(6) Many other research objectives based on the homogeneous composition and geometry of the composite.

APPENDIX I

Kramer's rule and determination of the upper critical field (H_{c2})

In his derivation of the flux pinning model [60,61] for high field, it is assumed that the strong pins do not break, but rather that the flux line lattice (FLL) shears plastically around these pins. This shear occurs when the shear stresses in the local FLL around these pins exceed the shear strength of the FLL.

When a superconductor carries the critical current, it was believed that a dynamic force was acting on the fluxoids moving with the average velocity, $\langle v \rangle$. In such situation, he equated the pinning power loss ($F_p \langle v \rangle$) and the overall rate at which elastic energy is stored in the FLL($2 E_s \wp \langle v \rangle / a_o$), an expression for the flux pinning force was obtained as

$$F_p = (2 \wp E_s)/a_o \qquad \text{(AI-1)}$$

where $\wp$ is the density of pins, E_s is the elastic energy stored in the FLL in a static interaction with a pin or local group of pins and a_o is the FLL parameter, which is inversely proportional to the square root of the applied magnetic field (i.e. $a_o \propto H^{-1/2}$).

To find out an appropriate expression for the stored energy per unit volume ($\wp E_s$), the system was simulated as one of typical problems in elasticity -- a fixed-ends-bar subjected to a uniform load. The pinning planes (zx-plane where the fluxoids aligned in z direction) were assumed as the fixed ends separated by a distance $1/\sqrt{\wp}$ in y-direction. The group of fluxoids between the pinning planes as the

continuum. Also the Lorentz force in x-direction took the place of the uniform force. Then the shear stress was found to be

$$\tau_{xy} = [(1/2\sqrt{\rho})-y]F_L \qquad \text{(AI-2)}$$

where F_L is the Lorentz force. Following some basic calculus with elasticity concept, the stored energy was expressed as

$$E_s = C_{66}/[24\pi^2(1-a_o\sqrt{\rho})^2] \qquad \text{(AI-3)}$$

where C_{66} is the shear moculus of the FLL, and others are the same as defined in equation (AI-1). Introducing equation (AI-3) into (AI-1), Kramer's expression for the dynamic pinning force was established as

$$F_p = \frac{1}{24\pi^2(1-a_o\sqrt{\rho})^2}\ \frac{C_{66}}{a_o} \qquad \text{(AI-4)}$$

In the above equation, the first factor is not a sensitive function with respect to the magnetic field. So it was assumed as a constant.

An expression for the shear modulus of the FLL near H_{c2} was theoretically derived and found to be proportional to the square of the difference between the upper critical field (H_{c2}) and the applied magnetic field (H) (i.e. $C_{66} \propto (H_{c2}-H)^2$) by R. Labush [62]. And a_o is proportional to $(\phi_o/H)^{1/2}$, where ϕ_o is the flux quantum. Substituting those expressions in equation (AI-4), Kramer's rule reduced to the well known practical form as

$$F_p = Jc \times H = C_s H^{1/2}(H_{c2}-H)^2 \qquad \text{(AI-5)}$$

where the exact value of H_{c2} should be measured from a magnetization experiment. If such experiment were not available, which is usually the case, the value can be approximated by extrapolating the data of J_c versus H for the fields near H_{c2}. A modified form of above equation as

$$(J_c H^{1/2})^{1/2} = C_s^{1/2}(H_{c2}-H) \qquad \text{(AI-6)}$$

is used for the purpose. In a $(J_c H^{1/2})^{1/2}$ versus H plot, H_{c2} can be found as the intercept on H-axis.

Kramer's model does predict the overall trend quite well. However there have been many superconductors which have slightly different behavior, especially at high field very near H_{c2}. It seems like a minor modification of the expression is necessary to describe the phenomena exactly.

For the modification, it is assumed that the basic idea of Kramer's shear deformation model, equation (AI-4), is an appropriate one. Then, the expression for the shear modulus (i.e. $C_{66} \propto (H_{c2}-H)^2$) is the only term to be modified. Phenomenologically, the critical current -- hence the critical current density and the flux pinning force -- should vanish at the H_{c2}. So an additional assumption can be made that the shear modulus should be expressed in terms of power of $(H_{c2}-H)$ but with various power indices depend on the superconductors (i.e. $C_{66} \propto (H_{c2}-H)^n$). The flux pinning force density for high field then can be written as

$$F_p = K_s H^{1/2}(H_{c2}-H)^n \qquad \text{(AI-7)}$$

where n is a constant to be determined from the experimental data. However, the situation is quite different from equation (AI-5), where H_{c2} can be extrapolated since the value of n is fixed as 2. But in equation (AI-7), it is not that simple, since n is an unknown. In this case, a numerical method seems to be a reasonable way to find the H_{c2} and the n simultaneously. If we note that all of the present $(J_c H^{1/2})^{1/2}$ versus H data bend upward at high field region, the power

should be greater than 2. And step-wise increasing the value of n from 2, a value of n, which fits for the most composites was found, and the values of H_{c2} for that curve were taken as the approximation.

APPENDIX II

Calculation of the grain boundary area per unit volume of filament as a function of the filament diameter

To have a rough idea on the flux pinning force density as a function of the filament diameter (D), it is useful to calculate the grain boundary area (which is known to be the only type of effective flux pinning center in Nb_3Sn) per unit volume of filament as a function of filament diameter.

Foremost, it is necessary to find an expression of the grain boundary area per unit volume, $\langle A \rangle$, in a material of infinitely large size. Next, an expression of $\langle A \rangle$ as a function of the filament diameter, $\langle A \rangle = f(D)$, should be found for the comparison between the filaments of various diameter. In the derivation of those expressions, it is assumed that the shape of a grain is a sphere with an average diameter, (d), which does not vary with the filament diameter. Then there are $\left[\frac{4}{3}\pi\left(\frac{d}{2}\right)^3\right]^{-1}$ grains per unit volume of material regardless the shape and the size.

For a material of infinitely large size, it is reasonable to assume that all the grain boundaries are inside the material. The the expression of $\langle A \rangle$ in this material is

$$\langle A \rangle_{inf.} = (1/2)\text{x(surface area of a grain)} \text{x(No. grains per unit volume)}$$

$$= \left(\frac{1}{2}\right) \times 4\pi\left(\frac{d}{2}\right)^2 \times \left[\frac{4}{3}\pi\left(\frac{d}{2}\right)^3\right]^{-1} = \frac{3}{d} \qquad \text{(AII-1)}$$

In the case of the filamentary material with filament diameter, (D), the length for unit volume is $[\pi(D/2)^2]^{-1}$. And the surface area for the length is

$$\langle S \rangle = (\pi D)(4/\pi D^2) = 4/D \qquad \text{(AII-2)}$$

However, in case of the fine filament, where D is about ten times of d, the surface of a filament can not be approximated as a smooth cylindrical surface. Rather the surface roughness, due to the individual grain should be considered. Since the smooth cylindrical surface area is 4/D, the number of grains on the surface (N_s) might be obtained by dividing the imaginative smooth surface area (i.e. 4/D) with the maximum cross-sectional area of a grain (i.e. $\pi(d/2)^2$). Then N_s is

$$N_s = 16/(\pi d^2 D) \qquad \text{(AII-3)}$$

And only the half surface of those grains constitutes the filament surface. Then the surface area of a fine filament might be expressed as

$$\langle S \rangle_{fine} = (N_s) \times (4\pi(d/2)^2) \times (1/2) = 8/D \qquad \text{(AII-4)}$$

Then the grain boundary area (inside a filament) per unit volume of fine filament is

$$\langle A \rangle = \langle A \rangle_{inf.} - (1/2)\langle S \rangle_{fine} = (3/d)-(4/D) \qquad \text{(AII-5)}$$

As derived in equation (AII-1), the maximum $\langle A \rangle$, which is the value in an infinitely large size material, is

$$\langle A \rangle_{max} = \langle A \rangle_{inf.} = 3/d \qquad \text{(AII-6)}$$

The 90% of $\langle A \rangle_{max}$ can be achieved with filament diameter, $D_{0.9}$, then

$$(0.9)\langle A \rangle_{max} = (3/d) - (4/D_{0.9})$$

and

$$D_{0.9} = (13.3)d \qquad \text{(AII-7)}$$

The value of $\langle A \rangle$ in the equation (AII-5) approachs to $\langle A \rangle_{max}$ asymptotically, when the filament diameter become large. On the other hand, the equation cannot be an appropriate approximation for ultrafine filament with the diameter several times of grain diameter. However, it is evident that the internal grain boundary area should approach to zero, in a monotonic fashion, as the filament diameter decrease. Then the internal grain boundary area per unit volume of filament as a function of the filament diameter can be schematically shown in Fig. AII.1.

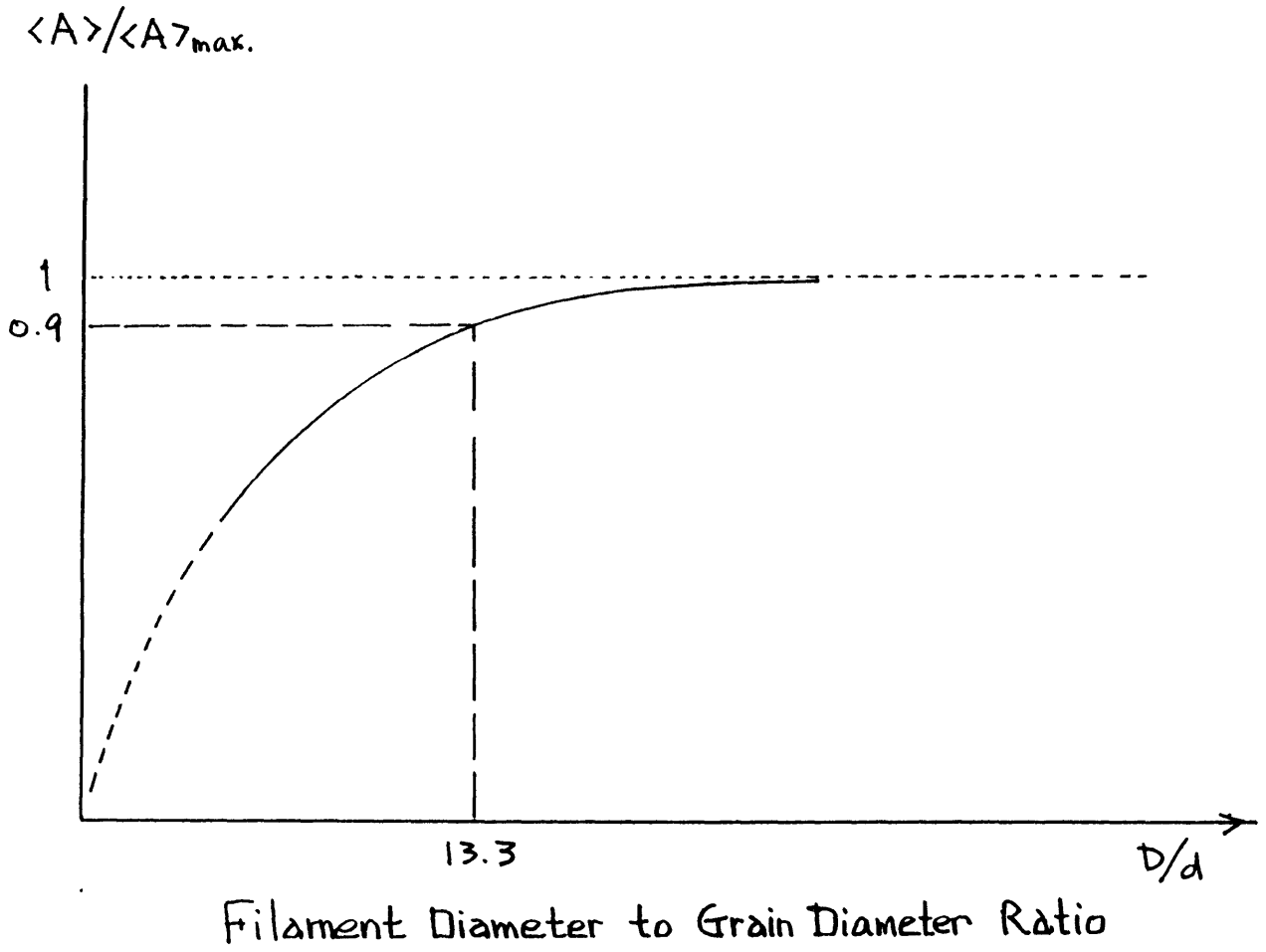

Fig. AII.1 A schematic illustration of the grain boundary area change depend on the filament diameter. $\langle A \rangle$; area of grain boundary in a unit volume of filament, $\langle A \rangle_{max}$; Maximum grain boundary area in a unit volume of bulk speciman, D;Filament diameter, d;grain diameter.

References

[1] J. E. Kunzler, E. Beuhler, F. S. L. Hsu and J. H. Wernick, Phys. Rev. Lett., 6 (1961) 89

[2] D. Dew-Hughes, Treatise on Materials Science and Technology, vol.14 Metallurgy of Superconducting Materials (eds. T.Luhman, D.Dew-Hughes), Academic Press, N.Y., (1979) 1

[3] M. N. Wilson, Superconductor Materials Science (eds. S. Foner and B. B. Schwartz), Plenum Press, (1981)

[4] A. R. Kaufman and J. J. Pickett, Bull. Am. Phys. Soc., 15 (1970) 833

[5] M. Suenaga and W. B. Sampson, Appl. Phys. Lett., 20 (1972) 443

[6] C. C. Tsuei, Science 180 (1973) 57

[7] R. Flukiger, S. Foner, E. J. McNiff, Jr., B. B. Schwartz, J. Adams, J. Forman, T. W. Eagar and R. M. Rose, IEEE Trans. on Magnetics, Mag-15 (1979) 689

[8] Y. Mashimoto, K. Yoshizaki, and M. Tanaka, Proc. 5th Inter. Cryog. Engin. Conf., Kyoto, Japan (1974) 332

[9] R. Ramdall, J. Wong, D. W. Dies, B. J. Shaw, and M. R. David, IEEE Trans. on Magnatics, Mag-11, (1975) 291

[10] Y. Koike, H. Shiraki, S. Marase, E. Suzuki and M. Ichihara, Appl. Phys. Lett. 29 (1976) 384

[11] W. K. Mcdonald, U.S. Patent No. 4,262,412

[12] W. K. Mcdonald, C. W. Curtis, R. M. Scanlan, D. C. Larbalestier, K. Marken and D. B. Smathers, IEEE Trans. on Magnetics, Mag-19 (1983) 1124

[13] R. M. Scanlan, W. A. Fietz and E. F. Koch, J. Appl. Phys., 46

(1975) 2244

[14] B. J. Shaw, J. Appl. Phys., 47 (1976) 2143

[15] J. Livingston, Phys. Stat. Sol. (a), 44 (1977) 295

[16] W. Schauer and W. Schelb, IEEE Trans. on Magnetics, Mag-17 (1981) 374

[17] T. Luhman, Treatise on Materials Science and Technology, vol.14 Metallurgy of Superconducting Materials (eds. T.Luhman, D.Dew-Hughes), Academic Press, N.Y., (1979), 221

[18] J. W. Ekin, Appl. Phys. Lett., 29 (1976) 216

[19] W. A. Pupp, W. W. Sattler and E. J. Saur, J. Low Temp. Phys., 14 (1974) 1

[20] C. B. Muller and E. J. saur, Rev. Mod. Phys., 36 (1964) 103

[21] S. Cogan, Ph.D. Thesis, M.I.T., Cambridge, Mass. (1979)

[22] S. Kwon, M.S. Thesis, M.I.T., Cambridge, Mass. (1982)

[23] J. Bevk, J. Harbison, F. Habbal, G. Wagner and A. Braginski, Appl. Phys. Lett., 36 (1980) 85

[24] M. Suenaga and D. Welch, Filamentary A15 Superconductor (eds. M. Suenaga and A. F. Clark), Plenum Press, N.Y., (1980) 131

[25] W. A. Backofen, Deformation Processing, Addison-Wesley Pub. Co., (1972) 77

[26] J. Sue, J. Verhoeven, E. Gibson, J. Ostenson and D. Finnemore, Acta Met. 29 (1981) 1791

[27] A. Bochvar, V. Sergeev, V. Kuznetsova, A. Nikulin, E. Klepatskaya and M. Fomishikin, Metallov. i Termi. Obra. Metallov., No.12 (1980) 44

[28] F. A. Shunk, Constitution of Binary Alloys, 2nd Suppl., McGraw-

Hill, NY, (1969) 370

[29] D. Dew-Hughes, Treatise on Materials Science and Technology, vol.14 Metallurgy of Superconducting Materials (eds. T.Luhman, D.Dew-Hughes), Academic Press, N.Y., (1979) 137

[30] D. Smathers and D. Larbalestier, to be published in J. Appl. Phys. (1984)

[31] T. H. Courtney, G. W. Pearsall and J. Wulff, TMS-AIME, 233 (1965) 212

[32] I. Wu, D. Dietderich, J. Holthuis, M. Hong, W. Hassenzahl and J. Morris, Jr., J. Appl. Phys., 54 (1983) 7139

[33] W. Schelb, J. Mat. Sci. 16 (1981) 2575

[34] A. W. West and R. Rawlings, J. Mat. Sci. 12 (1977) 1862

[35] B. Jacobson and R. Sinclair, New Developments and Applications in Composites (eds. D. Kuhlmann-Wilsdorf and W. Harrigan, Jr.) Proc. Symp. sponsored by the TMS-AIME Physical Met. and Composites Committees at the TMS-AIME Fall meeting in St. Louis, Missouri, Oct. 16-17 (1978) 204

[36] G. Rupp, E. J. McNiff and S. Foner, IEEE Trans. on Magnetics, Mag-17 (1981)370

[37] S. O. Hong and D. C. Larbalestier, IEEE Trans. on Magnetics, Mag-15 (1979) 784

[38] M. Suenaga, W. B. Sampson and T. S. Luhman, IEEE Trans. on Magnetics, Mag-17 (1981) 646

[39] H. Hillmann, H. Pfister, E. Springer, M. Wilhelm and K. Wohlleben, Filamentary A15 Superconductor (eds. M. Suenaga and A. F. Clark), Plenum Press, N.Y., (1980) 17

[40] G. Rupp, IEEE Trans. on Magnetics, Mag-15 (1979) 178

[41] J. Bevk, M. Tinkham, F. Habbal, C. J. Lobb and J. P. Harbison, IEEE Trans. on Magnetics, Mag-17 (1981) 235

[42] H. LeHuy, R. Roberge, J. L. Fihey, G. Rupp and S. Foner, IEEE Trans. on Magnetics, Mag-17 (1981) 261

[43] A. C. A. van Wees, P. Hoogendan and H. Veringa, IEEE Trans. on Magnetics, Mag-19 (1983) 556

[44] Zhou Lian, IEEE Trans. on Magnetics, Mag-19 (1983) 280

[45] J. Otubo, S. Pourrahimi, C. L. H. thieme, H. Zhang, B. B. Swartz and S, Foner, IEEE Trans. on Magnetics, Mag-19 (1983) 764

[46] S. F. Cogan, J. D. Klein, S. Kwon, H. Landis and R. M. Rose, IEEE Trans. on Magnetics, Mag-19 (1983) 917

[47] R. E. Schwall, G. M. Ozeryansky, D. W. Hazelton, S. F. Cogan and R. M. Rose, IEEE Trans. on Magnetics, Mag-19 (1983) 1135

[48] J. D. Verhoeven, J. J. Sue, E. D. Gibson, J. E. Ostneson and D. K. Finnemore, Acta Met., 31 (1983) 1233

[49] R. M. Scanlan, D. N. Cornish, J. P. Zbasnik, R. W. Hoard, J. Wong and R. Randall, Adv. Cryo. Eng. 26 (1980) 452

[50] J. Verhoeven, E. Gibson. F. Laabs, J. Ostenson and D. Finnemore, IEEE Trans. on Magnetics, Mag-19 (1983) 563

[51] D. K. Finnemore, J. D. Verhoeven, E. D. Gibson, J. E. Ostenson, IEEE Trans. on Magnetics, Mag-19 (1983) 259

[52] P. A. Sanger, E. Adam, E. Ioriatti and S. Richards, IEEE Trans. on Magnetics, Mag-17 (1981) 666

[53] E. Gregory, E. Adam. W. Marancik, P. Sanger and C. Spencer, IEEE Trans. on Magnetics, Mag-19 (1983) 47

[54] K. Agatsuman, K. Kaiho, K. Koyama, O. Kohno, Y. Ikeno and N. Sadakata, IEEE Trans. on Magnetics, Mag-19 (1983) 382

[55] A. DasGupta, C. Koch, D. Kroeger and Y. Chou, Phil. Mag. B, 38 (1978) 367

[56] R. D. Blaugher, R. E. Hein, J. E. Cox and R. M. Waterstrat, J. Low Temp. Phys., 1 (1969) 539

[57] M. Fahnle, J. Low Temp. Phys. 46 (1982) 3

[58] Hultgren, Selected values of the Thermodynamic Properties of Binary Alloys, ASM (1973) 1210

[59] J. Elen, J. Schinkel, A. van Wees, C. van Beijnen, E. Hornsveld, T. Stahlie, H. Veringa and A. Verkaik, IEEE Trans. on Mag., Mag-17 (1981) 1002

[60] E. J. Kramer, J. Appl. Phys., 41 (1970) 621

[61] E. J. Kramer, J. Appl. Phys., 44 (1973) 1360

[62] R. Labush, Phys. stat. sol., 32 (1969) 439